water

MDPI

Article

Future Wave Climate-Driven Longshore Sediment Transport and Shoreline Evolution along the Southwestern Black Sea

Büşra Başaran * and H. Anıl Arı Güner

Department of Civil Engineering, Faculty of Civil Engineering, Yıldız Technical University, Istanbul 34220, Turkey; aari@yildiz.edu.tr
* Correspondence: busrabasaran90@gmail.com

Abstract: This study investigates the future wave climate-driven longshore sediment transport (LST) and shoreline change on the Karasu Coast, situated on the southwestern coast of the Black Sea, under the RCP4.5 and RCP8.5 wave climate scenarios. Within the scope of this study, hourly deep sea wave data between 2021 and 2100, according to the RCP4.5 and RCP8.5, were used in order to predict future LST processes. Net and gross LST rates were computed using various empirical and numerical methods based on hourly wave parameters. By the conclusion of the study period after 80 years, the average net LST rates were obtained as 48,000 and 51,500 m^3/year in the RCP4.5 and RCP8.5, respectively, while the gross LST rates were 250,000 and 255,000 m^3/year. Due to the increase in wave height and period in both climate scenarios compared to the historical data, the average gross LST rates are projected to rise in the future. The reduction in swell wave heights, coupled with an increase in wind wave heights, compared to the past has led to a reduction in net LST. The results show that, after 80 years, LST will have increased 2.5 times more in the near future in comparison with the middle future for both scenarios.

Keywords: longshore sediment transport; shoreline change; Karasu Coast; future projection; empirical methods; LITDRIFT

check for updates

Citation: Başaran, B.; Arı Güner, H.A. Future Wave Climate-Driven Longshore Sediment Transport and Shoreline Evolution along the Southwestern Black Sea. *Water* **2024**, *16*, 1787. https://doi.org/10.3390/w16131787

Academic Editor: Achim A. Beylich

Received: 26 May 2024
Revised: 17 June 2024
Accepted: 19 June 2024
Published: 25 June 2024

Copyright: © 2024 by the authors. Licensee MDPI, Basel, Switzerland. This article is an open access article distributed under the terms and conditions of the Creative Commons Attribution (CC BY) license (https://creativecommons.org/licenses/by/4.0/).

1. Introduction

Coastal environments are dynamic systems shaped by complicated interactions between various factors, with wave climate standing out as the main driver of change. The study of variations in longshore sediment transport (LST) due to wave climate changes and shoreline change has emerged as an important field of research, particularly given the growing global concerns related to climate change, human activities, and the sustainable management of coastal areas. Waves, acting as powerful factors of geomorphic evolution, play a central role in shaping coastlines and influencing sediment transport along the shore. Coastlines, serving as dynamic boundaries between land and sea, are experiencing unique changes driven by the extensive effects of climate change. Shoreline dynamics are deeply influenced by shifts in climate patterns, sea-level rise, and extreme weather events, presenting a complex challenge for coastal regions globally. Understanding and assessing longshore sediment transport and coastline changes under the influence of climate change have become essential efforts in solving the interactions between environmental processes and human activities.

Various studies have been performed so far with the motivation of better comprehending future wave climate changes in LST and shoreline evolution. While some of these were LST studies [1–7], some of them were carried out to predict shoreline changes [8–18] is order to address the fact that long-term wave climate variations, influenced by regional climate change, present a complex issue affecting LST and coastline change. These studies suggest that climate change affects the LST mechanism through variations in wave characteristics and climate variability, with potential impacts on shoreline position and

orientation, and can aggravate coastal erosion in some regions while having a broadly neutral effect in others.

Chowdhury et al. [7] found that, while the drift direction of the Indian coast is expected to remain largely unchanged, the magnitude of longshore transport rates will vary, with some areas experiencing increased erosion and others accretion. Both swell and wind waves play a role in this complicated relationship, as demonstrated by Chowdhury and Behera [19], indicating that decreasing wave activity leads to a reduction in longshore sediment transport. The effect of climate change on LST is region-specific. On the central west coast of India, Chowdhury and Behera [20] observed a decreasing trend in longshore sediment transport due to the reduced swell generation in the Arabian Sea and Indian Ocean. A 5% decrease in transport in the same region has also been linked to reduced wave activity [19]. Similarly, Dastgheib et al. [5] observed substantial and spatially variable changes in longshore sediment transport rates along the coast of Vietnam, with some locations experiencing significant increases, highlighting the potential for climate change to alter wave characteristics and sediment transport rates, potentially leading to notable changes in the position and orientation of the shoreline. Adams et al. [1] demonstrated that variations in deep-water wave direction can alter LST patterns in Southern California, potentially increasing coastal erosion with increased cyclonic activity. Large-scale climate variability, as indicated by Splinter et al. [21], shows a strong correlation with longshore transport. Samaras and Koutitas [22] underscored the potential impact of climate change on sediment transport and coastal morphology in conjunction with watershed–coast systems, especially in extreme rainfall and wave events. Bonaldo et al. [3] emphasize that changing wave climates can lead to alterations in sediment transport processes, noting variations depending on the specific process and time scale. Overall, these studies collectively stress the importance of a comprehensive understanding of the various factors influencing longshore sediment transport in the context of regional climate change.

Climate change is driving significant changes in shorelines, with factors such as sea-level rise, changes in wave climate, and storm events playing key roles [9,23–25]. These changes are leading to increased coastal flooding, erosion, and land loss, creating a threat to the existence of natural beaches [26]. Along the coastline, the CoSMoS-COAST model of Vitousek et al. [26] predicts that 31–67% of Southern California beaches may erode by 2100. Therefore, future projections of wave climate are crucial in determining shoreline changes, with an increase in mean significant wave height and variations in wave frequency and wave direction expected [13]. Despite the challenges in predicting these changes, advancements in technology and a more integrated scientific focus are improving our understanding of shoreline change [25].

In the future, it will be necessary to observe the current climate changes to minimize the adverse effects that may occur due to climate change and predict how trends related to these changes will pan out in the future. To predict future climate conditions by understanding the current and past climate, mathematical models representing the components of the climate system and the interactions between these components are needed. Various scenarios are used in future climate predictions; they are obtained through models. A scenario is not a prediction of the future but defines possible alternative situations [27]. Currently, Representative Concentration Pathways (RCPs), selected from more than 40 scenarios developed under the IPCC in 2007, are used. There are several RCP scenarios, each associated with a specific radiative forcing level by the year 2100. Radiative forcing quantifies the disparity between incoming solar radiation and outgoing infrared radiation, primarily impacted by human activities such as the burning of fossil fuels. The commonly used RCP scenarios consist of RCP8.5, RCP6.0, RCP4.5, and RCP2.6, representing different levels of GHG concentrations and their associated radiative forcing. For example, the RCP2.6 assumes stringent mitigation efforts, leading to lower GHG concentrations and lower radiative forcing, while the RCP8.5 represents a high-emission scenario with significant climate change impacts [27]. This study conducted projection studies based on the RCP4.5 and RCP8.5 wave climate scenarios. The RCP8.5 is a high radiative forcing and concentration

pathway, while the RCP4.5 is a stabilization pathway, assuming that radiative forcing will be stabilized at 4.5 W/m^2 between 2100 and 2150.

This study concentrated on a specific region, namely the southwestern coast of the Black Sea, to examine the variation in the wave climate parameters in the future and their consequential effects on the mechanisms of coastal sediment transport. This initiative aims to provide insights into the complex dynamics of wave-driven processes and their impacts on coastal stability, thereby laying a base for informed decision-making and the adoption of sustainable coastal management practices.

Başaran and Arı Güner [28] investigated the changes observed in wave climate parameters, specifically wave height, period, and mean direction, along the coastal area of Karasu located on the southwestern coast of the Black Sea. Their investigation focused on understanding how these long-term changes influence the coastal sediment transport mechanisms in that particular region. The study identified the seasonal and year-to-year fluctuations within the existing nearshore wave climate and the associated coastal sediment transport mechanism along the Karasu Coast. Furthermore, their research aimed to emphasize the impacts of shifts in the nearshore wave climate on the transport of sediment along the coast. It is important to note that the present work is a follow-up study of Başaran and Arı Güner [28].

This paper makes a dual contribution. Initially, it evaluates the future influence of climate change on longshore sediment transport driven by waves along the Southwestern coast of the Black Sea. Notably, this assessment was the first to be conducted in this region employing climate projections. Secondly, to enhance the overall comprehension of the diverse effects of climate change, this study identifies the relationship between climate-induced longshore sediment transport and the resulting consequences observed in shoreline evolution as a second aspect.

The scope of the paper is as follows: in Section 2, the study area is presented, with the data used in the study detailed in Section 3. In Section 4, the results from the longshore sediment transport calculations, according to the RCP4.5 and RCP8.5 wave climate scenarios using three different empirical models and one numerical model, are given, followed by the results from the shoreline change model. Finally, the discussions are given in Section 5 and the conclusions are expressed in Section 6.

2. Study Area

The study area is the coastal area of Karasu, situated in the southwestern region of the Black Sea. The Black Sea is a semi-enclosed basin, bordered by the Caucasus to the north and northeast, Eastern Europe to the west, and Anatolia to the south. It spans between latitudes 40.910 N and 46.600 N and longitudes 27.450 E and 41.800 E. The Black Sea covers an area of 420,000 km^2, holds a water volume of 540,000 km^3, has an average depth of around 1.2 km, and reaches a maximum depth of 2.2 km [29,30]. The Karasu Coast is situated in the Marmara Region of Turkey, within the coastal segment belonging to the Karasu district of Sakarya province. Positioned in the southwestern region of the Black Sea, the Karasu Coast is situated between latitudes 30.300 N and 30.850 N and longitudes 41.225 E and 41.050 E. The study area encompasses a 25–30 km stretch along the western part of the Sakarya River mouth which possesses a sensitive shoreline under the influence of an active and highly complex sediment transport regime. Since cross-shore and longshore sediment transport systems are active along the Karasu Coast, the region stands as a unique domain where the dynamic forces of nature shape its geomorphology.

3. Data and Methodology

3.1. Wave Forcing

Future wave characteristics are obtained from the study of Islek et al. [31], which assessed the potential impact of climate change on the wave climate within a semi-enclosed sea, specifically the Black Sea, until the end of the 21st century. Wave data were generated using a third-generation wave model, which was driven by widely utilized reanalysis

data (Climate Forecast System Reanalysis). The hindcast wind fields were simulated by the five RCA4 (Rossby Centre Regional Atmospheric) models, namely MPI-ESM-LR, HadGEM2ES, IPSL-CM5A-MR, CNRM-CM5, and EC-EARTH [32]. According to the study of Islek et al. [32], the wind fields were compared to the CFSR reanalysis wind data to check the accuracy of wind fields during the historical period. The relative errors between the measured and modeled histograms are 9.22%, 10.52%, 9.76%, 9.05%, and 8.40% for MPI–ESM–LR, HadGEM2ES, IPSL–CM5A–MR, CNRM–CM5, and EC–EARTH, respectively [32]. For a detailed explanation of regional climate models and future wind characteristics in the Black Sea, we refer readers to Islek et al. [32]. The alterations in the wave climate pattern were examined through a comparative analysis between historical data from 1970 to 2005 and future projections for the periods 2021–2060 (near future) and 2061–2100 (middle future) under two distinct climate scenarios. The anticipated changes in mean wave characteristics indicated an increase in the near future under both RCP scenarios, with a more pronounced impact observed under the RCP8.5 scenario, particularly in the eastern basin. The middle future projections under the RCP8.5 scenario suggested more substantial alterations in annual mean values compared to those projected under the RCP4.5 scenario. Comparisons were conducted using both local and broader-scale analyses. Local comparisons involved assessing the model against measured buoy data from stations at Sinop (42°07′24″ N, 35°05′12″), Filyos (41°60′00″ N, 32°02′00″), Hopa (41°25′24″ N, 41°23′00″), Gelendzhik (44°30′27″ N, 37°58′42″), and Karaburun (41°21′00″ N, 28°41′00″) (Figure 1). Additionally, the entire study area was considered, with a comparison against modeled wave data generated using the Climate Forecast System Reanalysis (CFSR) wind fields covering the entire Black Sea. The relative errors between the modeled and measured station wave data histograms were 7.80%, 8.24%, 4.69%, 9.67%, and 9.36% for Gelendzhik, Sinop, Hopa, Karaburun, and Filyos stations, respectively. The results of the comparative analyses revealed a slightly better agreement for the EC-EARTH data [31] (see their Table 3). Consequently, an assessment of the near (2021–2060) and middle (2061–2100) future wave climate under both climate scenarios (RCP4.5 and RCP8.5) was conducted based solely on the RCA4 model, which exhibited more favorable alignment with the observed data. For a detailed account of the evaluation of regional climate models and future wave characteristics in the Black Sea, we refer readers to Islek et al. [31]. The wave data were extracted for the coordinates of the respective research area from the study of Islek et al. [31].



Figure 1. The geographic location of the study area and the locations of wave measurement stations (red pins).

Hourly deep-water wave forecast data for the period 2021–2100, representing the Karasu Region, were utilized to predict future coastal sediment transport processes based on the RCP4.5 and RCP8.5 climate scenarios. The impacts of these data were assessed for the near future (2021–2060) and the middle future (2061–2100) periods, explaining the region's wave climate in terms of monthly averages and seasonal variations.

3.2. Longshore Sediment Transport (LST)

LST, a fundamental process in coastal geomorphology, refers to the movement of sediment along the shoreline in response to waves and currents, contributing significantly to the evolution of coastal landforms. The complex interaction of natural forces, such as waves and tides, forms a dynamic system in which sediments are mobilized, transported, and deposited along the coastline. Several methods are employed to determine longshore sediment transport, each tailored to specific conditions and research objectives.

Empirical formulas employing four distinct methods are utilized to determine Longshore Sediment Transport (LST). The methods include the energy flux approach, current strength approach, dimensional analysis technique, and force equilibrium approach. LST, representing the sediment transport over a specific timeframe, is calculated based on waves from different directions within a defined period, necessitating the definition of the net LST rate. Coastal engineering studies have extensively utilized various formulas, with this study incorporating methods such as those of Kamphuis [33] and Kaczmarek et al. [34]. Kamphuis [33] validated through laboratory experiments chosen for their reliability in estimating LST, particularly for regions with low wave energy. Kaczmarek et al. [34] relied on radioisotopic measurements, which were selected due to the limited observations within the study region. Additionally, Bayram et al.'s [35] formula, considering multiple mechanisms, including wave-induced currents, wind, and tidal currents, was chosen for its comprehensive approach and suitability for numerically modeling shoreline change and longshore sediment transport. Consequently, these three empirical methods and a numerical model (LITPACK), elaborated on in the subsequent paragraphs, were employed in this study to provide a comprehensive understanding of LST from different perspectives. In Table 1, the formulas used in the empirical models are summarized. For a detailed account of the empirical models utilized in this study, we refer readers to Başaran and Arı Güner [28].

Table 1. Summary of the empirical models.

Method	Formula	Definition
Kamphuis [33]	$Q = 7.3 H_{sb}^2 T_p^{1.5} m_b^{0.75} D_{50}^{-0.25} sin^{0.6}(2\alpha_{bs})$	H_{sb}: significant wave height (m), T_p: peak wave period, m_b: slope of the beach in breaking zone, D_{50}: average grain size (m), α_{bs}: angle of breaking wave.
Kaczmarek et al. [34]	$Q = \begin{cases} H_b^2 V < 0.15 \text{ (low and medium wave climate)} \\ 0.023\left(H_b^2 V\right)\ [m^3/s]; \\ H_b^2 V > 0.15 \text{ (higher waves and storms)} \\ 0.00225 + 0.008\left(H_b^2 V\right)\ [m^3/s]; \end{cases}$ $V = 0.25 k_v \sqrt{\gamma_b g H_b} sin 2\theta_b$ $H_b = h_b \times \gamma_b,\ h_b = \lambda C^2/g,\ \lambda = \delta \times \lambda_a$ $\theta_b = arcsin\left(sin(\alpha_0)\sqrt{\lambda}\right)$ $\delta = 1 + 0.1649\varepsilon + 0.5948\varepsilon^2 - 1.6787\varepsilon^3 + 2.8573\varepsilon^4$ $\varepsilon = \lambda_a sin\alpha_0^2$	k_v: site-specific constant, γ_b: constant wave breaker parameter, λ: correction factor, δ: coupling coefficient, ε: transport coefficient.

Table 1. *Cont.*

Method	Formula	Definition
Bayram et al. [35]	$Q_{lst} = \frac{\varepsilon}{(\rho_s-\rho)(1-a)gw_s} F\overline{V}$ $\overline{V} = \frac{1}{x_b}\int_0^{x_b} Vdx = \frac{5}{32}\frac{\pi\gamma_b\sqrt{g}}{c_f} A^{3/2} sin\theta_b$ $A = \frac{9}{4}\left(\frac{w_s^2}{g}\right)^{1/3}, F_b = E_b C_{gb} cos\theta_b$ $E_b = \frac{1}{8}\rho g H_b^2, C_{gb} = \sqrt{g\frac{H_b}{\gamma_b}}$ $\varepsilon = \left(9.0 + 4.0\frac{H_{s,b}}{w_s T_p}\right) \times 10^{-5}, \varepsilon = \lambda_a sin\alpha_0^2$ $\lambda_a = [cos(\alpha_0)/\alpha]^{2/5}, \alpha = \left(\frac{C}{\sqrt{gH_s}}\right)^4 \left(\frac{C}{C_g}\right)\gamma_b^2$	ε: transport coefficient, $\overline{V}$: average longshore sediment current velocity in the surf zone, F: wave energy flux, A: porosity, w_s: fall velocity of the sediment.

Besides using empirical methods for LST estimation, this study also utilized a numerical model known as the LITPACK package. Developed by the Danish Hydraulic Institute [36], LITPACK is an integrated modeling system designed for assessing various coastal processes. It incorporates deterministic numerical modules, such as LITDRIFT, LITREN, LITLINE, LITPROF, and STP, providing a comprehensive approach to modeling the transportation of noncohesive sediment in waves and currents, littoral drift, shoreline change, and profile evolution. The LITDRIFT module within LITPACK, a deterministic numerical model, was specifically employed in this study to estimate LST rates [37]. This module conducts sediment budget analysis, crucial for coastal morphology studies, and models parameters like wave set-up, cross-shore wave height, and current along the coastal profile. By utilizing hydrodynamic and sediment transport models, the LITDRIFT module allows for the determination of longshore current and sediment transport, and annual sediment transport. Input data for the module include wave data from modeling results, bottom profiles, sediment characteristics, and initial coastlines. The LITDRIFT module considers numerous parameters influencing the sediment transport mechanism, including bottom roughness, bottom shapes, coastal geology, offshore bars, wind, currents, and various wave theories. The accurate determination of coastal parameters and the calibration of the model based on appropriate measurements are important for obtaining reliable results that align with natural conditions.

Upon analyzing the sediment characteristics along the Karasu Coast, it becomes evident that the seabed sediment is very well classified and falls under the category of medium sand, devoid of cohesive properties. In order to ascertain the sediment properties along the Karasu shoreline, measurements were conducted, involving the collection of sediment samples from various cross-sections. At each cross-section, three sediment samples were obtained from depths of −5 m, −10 m, and −15 m, respectively. The particle-size distributions of the sediment specimen were assessed through the sieving method.

Derived from measurements taken at the site, the values employed for the median grain diameter (D_{50}) and geometric standard deviation, $\sigma_g = \sqrt{D_{84}/D_{16}}$), were 0.38 mm and 1.336, respectively.

3.3. Shoreline Change

Shoreline change analysis was conducted using the LITLINE module, a component of the LITPACK 2016 software package, which employs a well-known numerical modeling system. This model is rooted in the one-line theory for shoreline change modeling [38].

Specifically, LITLINE, the focus of this study, calculates shoreline changes over a specified period by considering temporally and spatially changing longshore sediment transport. The module determines the position of the coastline according to the input data, representing the wave climate as a time series. Although rooted in the one-line theory, the model assumes that the cross-shore profile remains unchanged during erosion and accretion, with slight adjustments made for accurate representation.

The representation of coastal morphology is exclusively based on the position of the coastline in the cross-shore direction and the profile of the coast at a specific longshore location. In this study, the LITLINE module was employed to investigate alterations in shoreline attributed to natural factors, protected structures, and the examination of strategies for shoreline recovery through artificial beach nourishment. The utilization of LITLINE is supported by the continuity equation for sediment volumes Q(x), as outlined in DHI, the LITLINE User Guide [38]:

$$\frac{\partial y_c(x)}{\partial t} = -\frac{1}{h_{act}(x)}\frac{\partial Q(x)}{\partial x} + \frac{Q_s(x)}{h_{act}(x)\Delta x} \quad (1)$$

where $y_c(x)$ is the position of the shoreline; Q(x) indicates the longshore sediment transport volume; t denotes time; x represents the longshore position; $h_{act}(x)$ denotes the height of the active cross-shore profiles; Δx signifies the longshore discretization step; and $Q_s(x)$ represents the source/sink term expressed in volume.

The computation of $h_{act}(x)$ and $Q_s(x)$ is based on user-defined specifications, where Q(x) is obtained from the surf zone sediment transport rate table. Starting from the initial shoreline position $y_{initial}(x)$, the temporal development is ascertained by solving the provided equation, as detailed in [38]. The continuity equation of sediment budget is addressed using an implicit Crank–Nicholson scheme, revealing the progression of the shoreline position over time. Module input data encompass topographical conditions such as shoreline position, offshore contours, dune characteristics, and the cross-shore profile along the beach. These parameters are defined within a coordinate system where the *x*-axis aligns quasi-parallel to the initial shoreline, and y is perpendicular to x, oriented towards the sea.

Additional input data for LITLINE include sediment characteristics (mean sediment diameter D_{50}, geometrical spreading), hydrological conditions (medium sea level with storm surge and tide), current conditions, and wave conditions (depicted in a 2D wavetable containing wave height, wave periods, and wave directions). Besides the automatically calculated wave-induced current, other variables like speed, direction, and parameters related to the structural parameters (position, apparent dimensions, number, and factors for active dimensions of coastal structures like groins, jetties, revetments, and breakwaters) were entered directly into the program. The model's results are presented in graphic and tabular formats, including the depth of the topographic bed (m), shoreline position in time series (m), accretion of sediment transport rate (m^3), sediment transport rate (m^3/day), and sediment transport rate unit (m^3/m).

The essential inputs required for running the LITLINE model involve the wave climate, initial coastline, sediment characteristics, and bathymetry. Bathymetry is represented as a cross-shore profile, originating from offshore and extending up to two or three grid points into the beach. The coastal segment under consideration in this study is a linear sandy coast spanning approximately 25.2 km and modeled using 2521 grid cells, each measuring 10 m in length. At approximately equal intervals along this distance, six profiles were defined as inputs for the model. The shoreline normal of the study area inclines at an angle of 17°~20° to the east concerning true north.

The LITLINE model underwent calibration and validation through the utilization of satellite images. Shoreline changes derived using the LITLINE module were compared with shorelines extracted directly from the satellite images. The PLEIADES satellite images employed in this study possess an 11-byte radiometric solution and a resolution of 0.7 m. The calibration of the numerical model is explained in detail in Başaran and Arı Güner [28].

4. Results

4.1. Assessment of Future Wave Climate

Upon analyzing 80-year averages of wave parameters, the significant wave height (H_s), peak wave period (T_p), and mean wave direction (D_m) were observed as 0.94 m, 5.74 s,

and 15.2° (N-NNE) for the RCP4.5 and 0.95 m, 5.75 s, and 17.5° (N-NNE) for the RCP8.5 during the same period.

Figure 2 illustrates the 80-year monthly averages (averages of 80 January months, for instance) for significant wave height (H_s), peak wave period (T_p), and mean wave direction (D_m). Additionally, these figures provide seasonal variations in the monthly average wave parameters for total waves, swell waves, and wind waves. For the whole study period (80 years), the annual average heights of swell waves and wind waves ($H_{s,swell}$) and ($H_{s,wind}$) were determined to be 0.88 m and 0.24 m, respectively, for the RCP4.5, and 0.88 m and 0.23 m, respectively, for the RCP8.5. From the results, it can be noticed that the annual average significant wave height of wind waves was significantly lower compared to swell waves, attributed to the significant fetch distances (>600 km) influencing the generation of swell waves within the Black Sea Basin, as emphasized in Başaran and Arı Güner [28].

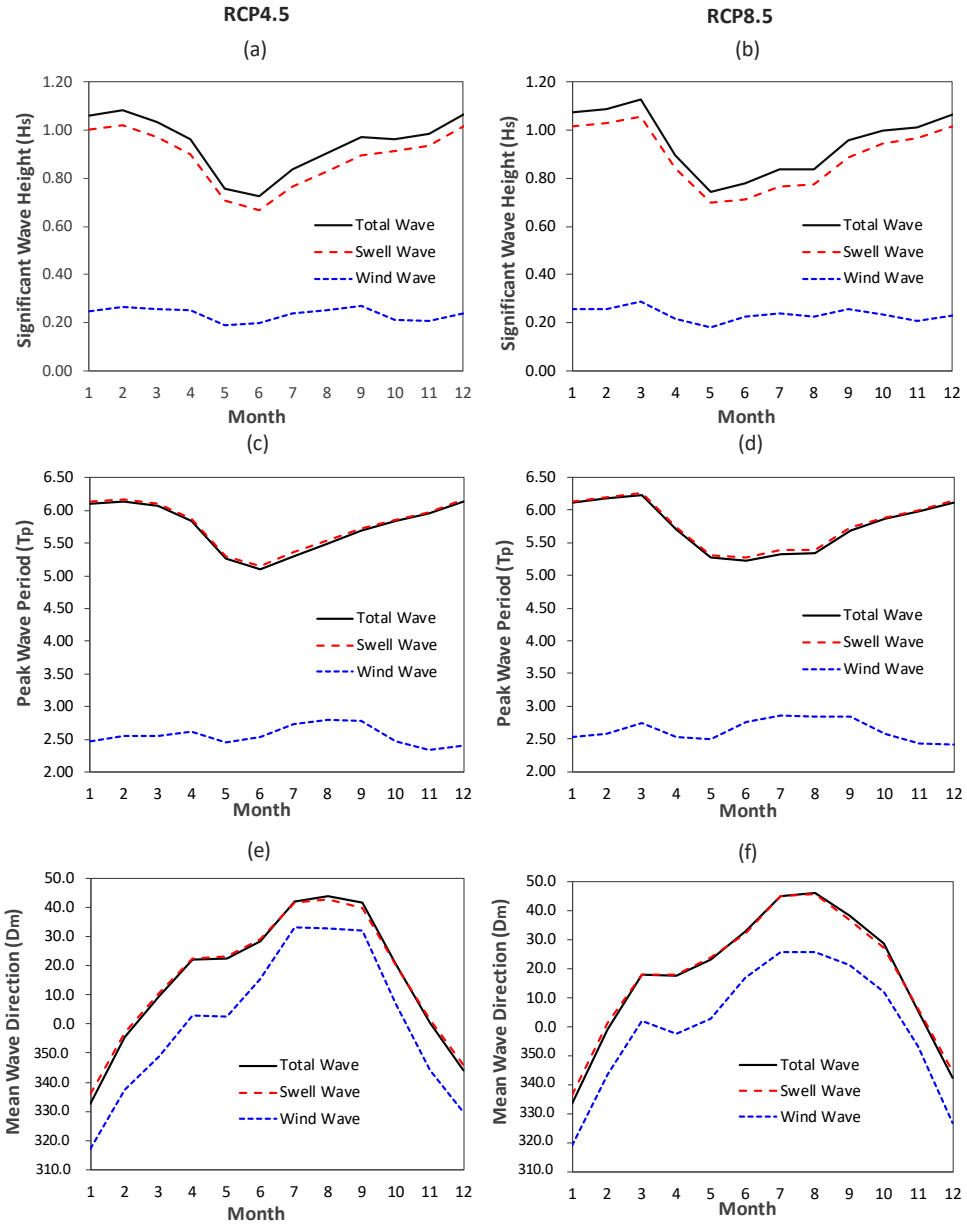


Figure 2. Monthly changes in H_s, T_p, and D_m values of the total, swell, and wind waves according to the RCP4.5 and RCP 8.5 wave climate scenarios; significant wave height (H_s): (**a**) RCP4.5 and (**b**) RCP8.5. Peak wave period (T_p): (**c**) RCP4.5 and (**d**) RCP8.5. Mean wave direction (D_m): (**e**) RCP4.5 and (**f**) RCP8.5.

Upon reviewing Figure 2, it becomes evident that wave heights increase during autumn and winter, while they decrease during spring and summer across both climate scenarios. Consequently, longshore sediment transport is anticipated to be higher during autumn and winter, and lower during spring and summer, for both RCP4.5 and RCP8.5 scenarios. These findings will become apparent upon examination of Figure 4.

For the RCP4.5 and RCP8.5 climate scenarios, the 80-year trends of significant wave height (H_s), peak wave period (T_p), and mean wave direction (D_m) parameters for total, swell, and wind waves are presented in Figure 3. The wave parameters were examined for the periods 2021–2060 and 2061–2100, representing the near and middle future, respectively. Upon analyzing the data, it can be observed that the swell waves are nearly equal to the total wave values, while the wind waves contribute much less to the total waves. Trend analyses from Figure 3 lead to the results given in Table 2.

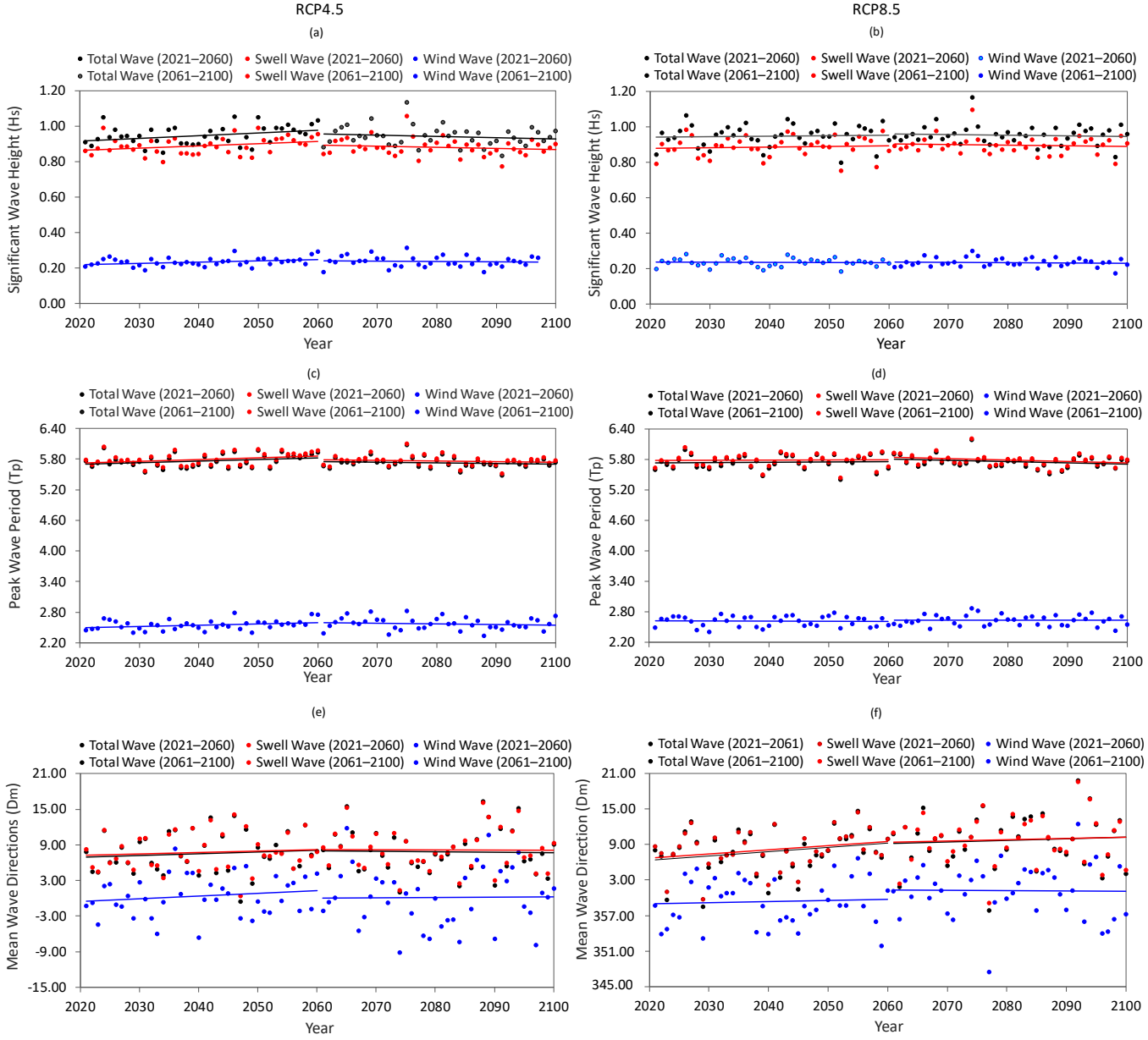


Figure 3. Annual changes in the RCP4.5 and RCP8.5 wave climate parameters in the near and middle future; significant wave height (H_s): (**a**) RCP4.5 and (**b**) RCP8.5. Peak wave period (T_p): (**c**) RCP4.5 and (**d**) RCP8.5. Mean wave direction (D_m): (**e**) RCP4.5 and (**f**) RCP8.5.

Table 2. Results of the trend analyses shown in Figure 3.

RCP4.5 Wave Climate Scenario			
	For 80 Years (2021–2100)		
Wave Parameters	**Total Wave**	**Swell Wave**	**Wind Wave**
Significant Wave Height	0.42% increase	1.10% increase	4.40% increase
Peak Wave Period	0.52% decrease	0.52% decrease	2.20% increase
Mean Wave Direction	0.60° shift to ESE	0.80° shift to ESE	0.30° shift to ESE
	Near Future (2021–2060)		
Wave Parameters	**Total Wave**	**Swell Wave**	**Wind Wave**
Significant Wave Height	6.50% increase	5.80% increase	9.90% increase
Peak Wave Period	2.20% increase	2.30% increase	4.20% increase
Mean Wave Direction	1.10° shift to ESE	1.00° shift to ESE	1.70° shift to ESE
	Middle Future (2061–2100)		
Wave Parameters	**Total Wave**	**Swell Wave**	**Wind Wave**
Significant Wave Height	2.60% decrease	3.00% decrease	2.50% decrease
Peak Wave Period	0.90% decrease	0.93% decrease	1.70% decrease
Mean Wave Direction	0.40° shift to WNW	0.20° shift to WNW	0.25° shift to ESE
RCP8.5 Wave Climate Scenario			
	For 80 Years (2021–2100)		
Wave Parameters	**Total Wave**	**Swell Wave**	**Wind Wave**
Significant Wave Height	0.74% increase	1.50% increase	1.70% increase
Peak Wave Period	0.17% decrease	0.35% decrease	0.76% increase
Mean Wave Direction	3.60° shift to ESE	3.50° shift to ESE	2.80° shift to ESE
	Near Future (2021–2060)		
Wave Parameters	**Total Wave**	**Swell Wave**	**Wind Wave**
Significant Wave Height	1.10% increase	1.70% increase	1.27% decrease
Peak Wave Period	0.40% increase	0.30% increase	0.11% decrease
Mean Wave Direction	2.70° shift to ESE	2.70° shift to ESE	1.0° shift to ESE
	Middle Future (2061–2100)		
Wave Parameters	**Total Wave**	**Swell Wave**	**Wind Wave**
Significant Wave Height	1.60% decrease	1.30% decrease	6.85% decrease
Peak Wave Period	1.70% decrease	1.70% decrease	0.53% decrease
Mean Wave Direction	1.10° shift to ESE	0.30° shift to ESE	0.30° shift to WNW

Examining the significant wave heights for total waves at the end of 80 years, it is evident that wave height increased in both scenarios, with a higher increase in the RCP8.5 scenario. After reviewing Table 2, it becomes evident that the significant wave height of total waves exhibits rises of 0.42% and 0.74% under the RCP4.5 and RCP8.5 climate scenarios, respectively. Therefore, it can be expected that there will be a higher amount of LST in the RCP8.5 scenario with higher wave heights compared to the RCP4.5 scenario. However, when the peak wave periods are examined, a decrease is observed in both scenarios for both total and swell waves, while the periods of wind waves show an increase. The reduction in the peak wave period was found to be 0.52% under the RCP4.5 climate scenario, while it was observed to be 0.17% under the RCP8.5 climate scenario. On the other hand, at the end of the 80 years, notable differences emerge in mean wave directions between the RCP8.5 and RCP4.5 scenarios, with the former exhibiting more significant changes. In the RCP8.5 scenario, waves tend to approach the shore at angles closer to the shoreline's normal, shifting by 3.6° eastward compared to the RCP4.5 scenario, which shows a 0.6° eastward shift. These angle changes may seem minor, but as indicated by Başaran and Arı Güner [28], these minor changes have a significant effect on the net and gross LST rates. Based on this study, 0.25° and 2° increases in incident wave direction over a 40-year historical period resulted in average decreases of 4.4% and 39.2% in annual net

longshore sediment transport rates, respectively. Conversely, reductions in incident wave direction by 0.25° and 2° led to increases in annual net longshore sediment transport rates by 4.0% and 31.7%, respectively [28].

According to the RCP4.5 scenario, in the near future (between 2021 and 2060), the significant wave height and peak wave period of the total wave (swell + wind) show increases of 6.5% and 2.2%, respectively, while the mean wave direction slightly shifts 1.1° eastward, indicating that the incident angle of the waves is shifting towards the shoreline's normal. In the near future, under the RCP8.5 scenario, there is a 1.1% increase in the significant wave height and a 0.4% increase in the peak wave period of the total wave (combination of swell and wind). Simultaneously, the mean wave direction shifts eastward by 2.7°, signifying a change in the incident angle of the waves towards the shoreline normal. Considering these results, it is expected that, in the near future, based on the increasing rates in wave heights, the net LST rate for the RCP4.5 scenario between 2021 and 2060 will have a greater increasing trend compared to the RCP8.5 scenario. Moreover, in the RCP8.5 scenario, towards the end of the near future (by 2060), the mean wave direction relative to the shoreline's normal is less compared to the RCP4.5 scenario, expressing that the waves are approaching the coast more perpendicularly, which will result in a slightly less increasing trend in the net LST rate.

For the RCP4.5 scenario, in the middle future (2061–2100), the significant wave height and peak wave period of the total wave (swell + wind) show decreases of 2.6% and 0.9%, respectively, while the mean wave direction will shift 0.4° westward, increasing the angle with the shoreline's normal. In the middle future under the RCP8.5 scenario, there is a decline of 1.6% in the significant wave height and a 1.7% decrease in the peak wave period of the total wave (combination of swell waves and wind waves), while the mean wave direction shifts 1.1° eastward, slightly decreasing the angle with the shoreline's normal. Considering these results, it is expected that, between 2061 and 2100, both the RCP4.5 and RCP8.5 scenarios will lead to a decreasing trend in the net LST rate.

4.2. Assessment of Future Longshore Sediment Transport

To predict future coastal sediment transport processes, hourly deep-sea wave data representing the Karasu region for the years 2021–2100 under the RCP4.5 and RCP8.5 climate scenarios were utilized using the methods of Kamphuis [33], Kaczmarek et al. [34], Bayram et al. [35], and LITDRIFT. The impacts of these data on the changes in coastal sediment transport quantities are evaluated for the near and the middle future, along with an explanation of the region's wave climate concerning monthly averages and seasonal variations.

Total waves (swell + wind) reach the coast from the west of the coastline's normal during November-March, while they reach the coast from the east of the coastline normal during April-October (Figure 2). Therefore, during certain periods of the year (April–October), a negative net LST occurs towards the upstream (western side of the Karasu Coast), while, during some periods of the year (November–March), a net LST occurs towards the downstream (eastern part of the study area). As evident from Figure 2, swell waves, which exhibit almost the same seasonal variation as the total wave data, contribute to LST in both westward and eastward directions in the study area. At certain periods of the year, these swell waves originate from the west of the coast, while, at other times, they propagate from the east, forming LST along the shoreline in both directions.

The seasonal variations in net LST and gross LST rates due to swell waves and wind waves are also shown for two different scenarios in Figure 4. While the net LST rates due to swell are high in the winter months, they are much lower in the spring and summer months for both climate scenarios. Upon examining Figure 4, it becomes apparent that the seasonal fluctuations in longshore sediment transport rates correlate directly with the seasonal variations in the wave parameters depicted in Figure 2. In the spring and summer months (between April and October), the direction of LST along the coastline changes, moving upstream. The contribution of the wind waves to the net and gross LST rates is

minimal throughout the whole year for both climate scenarios. During the winter months, notably November, December, and January, the wind wave-induced longshore sediment transport rate demonstrates minimum values. Conversely, it particularly peaks in July and August. Furthermore, it can be observed that the wind wave-induced total sediment transport rate is relatively low and in the opposite direction to the total swell wave-induced sediment transport, as illustrated in Figure 4.

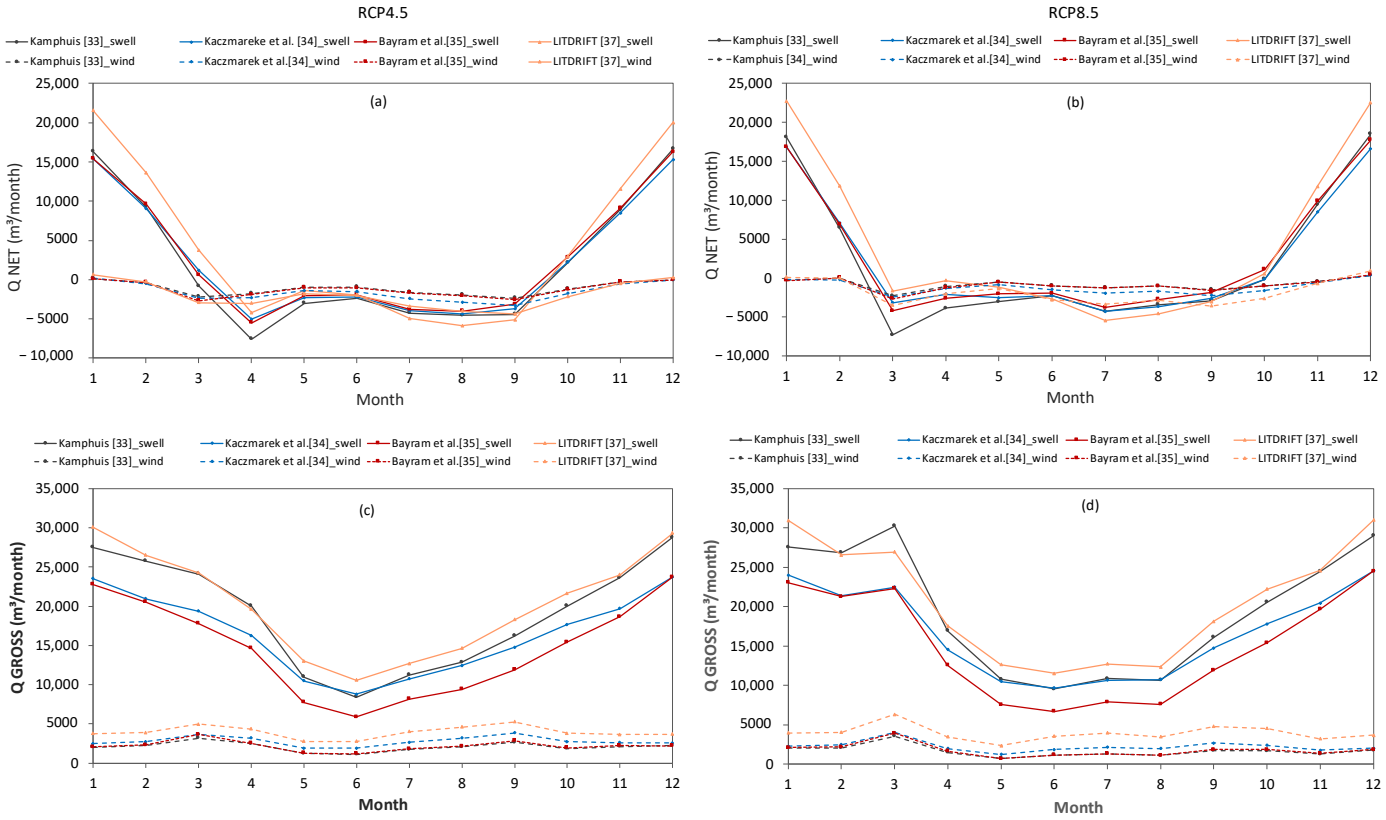


Figure 4. Seasonal changes in swell and wind wave-induced longshore sediment transport rates according to the RCP4.5 and RCP8.5 scenarios. Q_{NET}: (**a**) RCP4.5 and (**b**) RCP8.5. Q_{GROSS} (**c**) RCP4.5 and (**d**) RCP8.5.

To determine the changes in annual LST rates between 2021 and 2100, the average amounts for each year were calculated and graphed as the net and gross LST rates according to the RCP4.5 and RCP8.5 scenarios, respectively. The trend lines in Figure 5 clearly illustrate the significant variation in LST over the years. Figure 5a,b show the positive and negative LST rates for the RCP4.5 and RCP8.5 climate scenarios, respectively. While positive net longshore sediment transport occurs towards the ESE (downstream) direction, negative net longshore sediment transport occurs towards the NWN (upstream) direction.

Upon examining the negative and positive LST values together, as shown in Figure 5a, the average net LST rate according to the RCP4.5 is found to be around 0.48×10^5 m^3/year. The net LST rates for each method are 0.48×10^5, 0.38×10^5, 0.51×10^5, and 0.54×10^5 m^3/year for Kamphuis [33], Kaczmarek et al. [34], Bayram et al. [35], and LITDRIFT, respectively. When examining the negative and positive LST values according to the RCP8.5 together, as shown in Figure 5b, the average net LST rate is observed around 0.52×10^5 m^3/year for all methods. The net LST rates for each method are 0.52×10^5, 0.41×10^5, 0.55×10^5, and 0.58×10^5 m^3/year for Kamphuis [33], Kaczmarek et al. [34], Bayram et al. [35], and LITDRIFT, respectively.

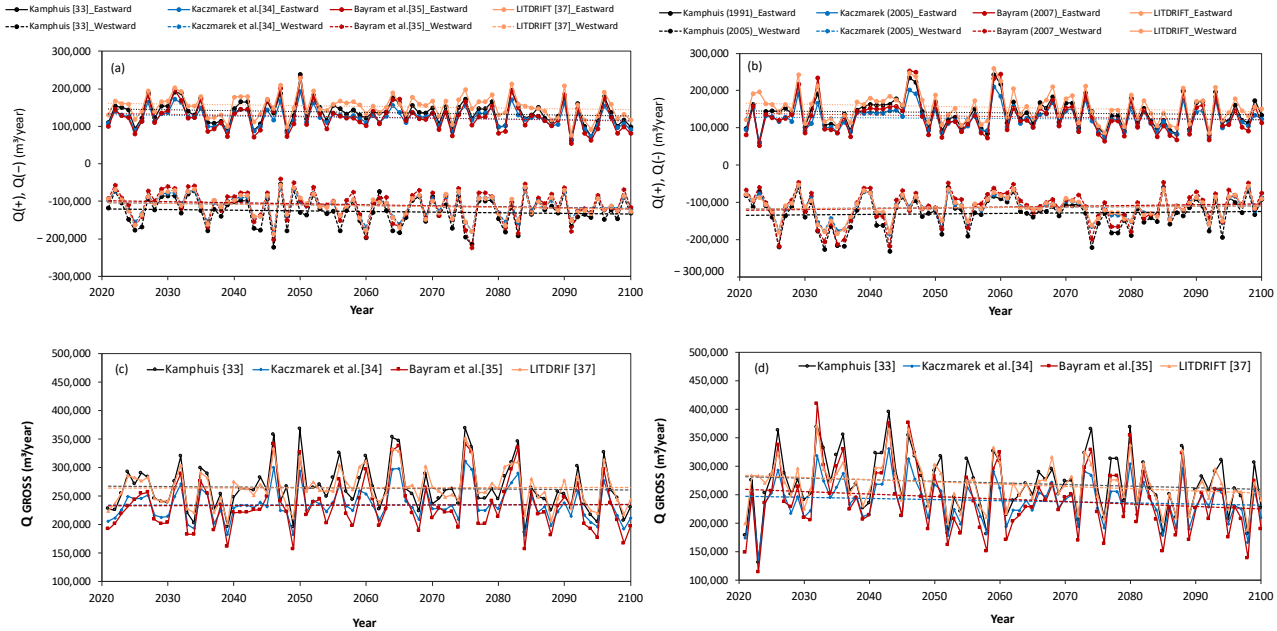


Figure 5. Annual changes in the net and gross sediment transport rates obtained from four different methods according to the RCP 4.5 and RCP8.5 scenarios: (**a**,**b**): Q_{NET} and (**c**,**d**): Q_{GROSS}.

According to the RCP4.5 scenario, the annual gross LST rates vary between 1.57 and 3.69 × 10^5 m^3/year, with an average of around 2.50 × 10^5 m^3/year for all methods. The gross LST rates for each method are 2.64 × 10^5, 2.35 × 10^5, 2.34 × 10^5, and 2.65 × 10^5 m^3/year for Kamphuis [33], Kaczmarek et al. [34], Bayram et al. [35], and LITDRIFT, respectively (Figure 5c). According to the RCP8.5 scenario, the annual gross LST rates range from 1.14 to 4.67 × 10^5 m^3/year, with an average of around 2.56 × 10^5 m^3/year for all methods. The gross LST rates for each method are 2.72 × 10^5, 2.40 × 10^5, 2.43 × 10^5, and 2.69 × 10^5 m^3/year for Kamphuis [33], Kaczmarek et al. [34], Bayram et al. [35], and LITDRIFT, respectively (Figure 5d).

When analyzing Figure 5a,b, regardless of direction, a decrease of approximately 400 m^3/year and 50 m^3/year (average on an annual basis) in the net LST rate can be observed at the end of the 80-year period for the RCP4.5 and RCP8.5 scenarios, respectively.

As depicted in Figure 5a,b, the net longshore sediment transports for both RCP4.5 and RCP8.5 scenarios were assessed separately, considering the direction over the 80-year study period. Upon analyzing Figure 5a, it was noted that the longshore sediment transport rates towards ESE (downstream) decrease by 13.0%, 4.4%, 14.5%, and 11.3% according to the methods of Kamphuis [33], Kaczmarek et al. [34], Bayram et al. [35], and LITDRIFT, respectively. Conversely, the same figure that longshore sediment transport towards WNW (upstream) increases by 18.0%, 17.6%, 20.0%, and 17.6% for these four methods, respectively.

Upon examining Figure 5b, it is evident that the longshore sediment transport rate towards ESE (downstream) demonstrates decreases of 6.2%, 7.0%, 14.3%, and 15.5% for the Kamphuis [33], Kaczmarek et al. [34], Bayram et al. [35], and LITDRIFT methods, respectively. Similarly, when inspecting the same figure for longshore sediment transport towards WNW (upstream), decreases of 9.5%, 7.6%, 14.2%, and 7.6% are observed for these four methods, respectively.

Examining Figure 5c, for the RCP4.5 scenario, gross longshore sediment transport rates show a decrease of 3.3%, an increase of 1.3%, an increase of 2.2%, and an increase of 1.1% for the Kamphuis [33], Kaczmarek et al. [34], Bayram et al. [35], and LITDRIFT methods, respectively. The average increase in gross longshore sediment transport rates over the 80-year study period is found to be 0.33%. When examining Figure 5d for the RCP8.5 scenario, gross longshore sediment transport rates show decreases of 7.0%, 5.6%, 13.1%, and 11.2% for the Kamphuis [33], Kaczmarek et al. [34], Bayram et al. [35], and LITDRIFT

methods, respectively. The average reduction in gross transport rates over the 80-year study period is found to be 9.2%. The decline in longshore sediment transport (LST) for the RCP8.5 climate scenario correlates directly with waves approaching the shore at angles closer to the shoreline normal, reaching the coast more perpendicularly. Consequently, it is evident that the wave incidence angle plays a significant role in influencing longshore sediment transport, underscoring its effectiveness as a key parameter.

The total net LST rate calculated for the study region, without distinguishing between swell and wind sources, is approximately 48,000 m^3/year (the average of three different empirical methods and one numerical method) for the RCP4.5 scenario and approximately 51,500 m^3/year for the RCP8.5 scenario. The gross LST rates are approximately 250,000 m^3/year for the RCP4.5 scenario and around 255,000 m^3/year for the RCP8.5 scenario. It was determined from Figure 5 that the net and gross longshore sediment transport rates obtained in the RCP8.5 climate scenario were 1.08 and 1.02 times greater, respectively, compared to the RCP4.5 scenario. The net LST and gross LST rates calculated according to the Kamphuis [33], Kaczmarek et al. [34], Bayram et al. [35], and LITDRIFT [37] methods are summarized in Table 3 below.

Table 3. Net and gross LST rates according to four various methods.

RCP4.5 Wave Climate Scenario				
Sediment Transport Rate (m^3/year)	**Kamphuis [33]**	**Kaczmarek et al. [34]**	**Bayram et al. [35]**	**LITDRIFT [37]**
NET	48,500	38,400	51,500	53,800
GROSS	264,000	235,200	234,850	264,600
RCP8.5 Wave Climate Scenario				
Sediment Transport Rate (m^3/year)	**Kamphuis** [33]	**Kaczmarek et al.** [34]	**Bayram et al.** [35]	**LITDRIFT** [37]
NET	51,700	41,150	54,500	58,350
GROSS	270,600	239,150	242,000	268,500

According to the results obtained for the net LST rates, the methods of Bayram et al. [35], Kaczmarek et al. [34], and Kamphuis [33] show results that can be considered consistent with each other, while the LITDRIFT model tends to predict larger net LST rates compared to the empirical methods (Table 3). When the empirical methods are evaluated among themselves, the Bayram et al. [35] method yields a larger net LST rate compared to the other two methods. It is believed that the difference arises from the fact that the Bayram et al. [35] approach, unlike the other methods, considers not only wave-induced currents but also wind and tidal currents in the coastal sediment transport calculation, resulting in a larger net coastal sediment transport rate.

The gross LST rates predicted for the Karasu Region between 2021 and 2100 were examined in separate 40-year periods for the near and middle futures, and trend analyses for all methods in these periods were conducted (Figure 6). In the near future period, representing 2021–2060, based on the RCP4.5 scenario, gross LST rates show an average increase of 10.4%, while for the same period based on the RCP8.5 scenario, gross LST rates show an average increase of 1.75%. However, during the middle future period, defined within 2061–2100, gross LST rates based on the RCP4.5 scenario show an average decrease of 12.7%, while for the same period based on the RCP8.5 scenario, gross LST rates show an average decrease of 8.0%. Therefore, when evaluating the period between 2021 and 2100, it can be said that the gross LST rates for the near and middle futures in the RCP4.5 scenario can almost balance each other, while in the RCP8.5 scenario, a significant decrease in transport rates is expected in the middle future, and an equilibrium situation is not anticipated. However, when Figure 6 is examined, it can be seen that the rates of change in near and middle future LST for the RCP4.5 climate scenario are much larger compared to the RCP8.5 climate scenario, contrary to the 80-year changes.

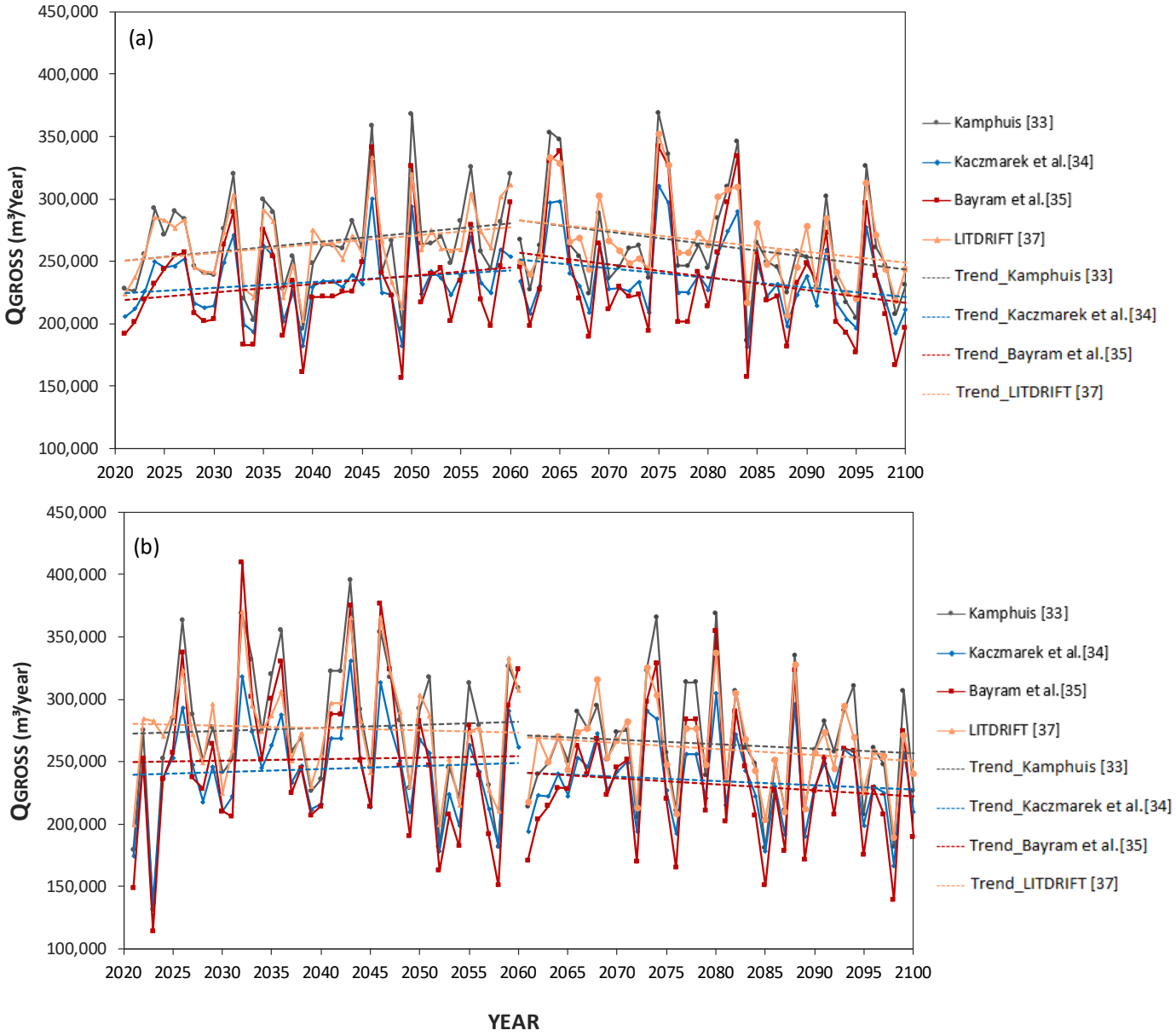


Figure 6. Annual changes in the gross longshore sediment transport rates according to the RCP4.5 and RCP8.5 scenarios for the near (2021–2060) and middle futures (2061–2100): (**a**) RCP4.5 and (**b**) RCP8.5.

The inter-annual variation in the average longshore sediment transport (LST) rates was examined for the near future (2021–2060), middle future (2061–2100), and the entire study period (2021–2100) under both the RCP4.5 and RCP8.5 scenarios. The long-term trend values, calculated using linear regression, are shown in Table 4. Gross LST values, for which linear regression analysis was performed, were calculated by averaging the values obtained from four methods (Kamphuis [33], Kaczmarek et al. [34], Bayram et al. [35], and LITDRIFT) for each year. The significance of calculated trends was assessed by Student's *t*-test, as explained by Santer et al. [39], (Appendix A), and the results are also provided in Table 4. Figure 7 illustrates the inter-annual trend lines with a 90% confidence level. Examining the trend lines reveals significant changes in the middle future for both climate scenarios. In the near future scenario, there is a significant change in the RCP4.5 climate scenario, whereas no significant trend (NST) is observed in the RCP8.5 climate scenario. When evaluating the gross LST rates over the entire 80-year period, without distinguishing

between the near and middle future, significant changes are observed in the RCP8.5 climate scenario, while the RCP4.5 climate scenario shows no significant trend (NST).

Table 4. Long-term trends in the LST rates according to the RCP4.5 and RCP8.5 wave climate scenarios.

Near Future (2021–2060)				
Scenario	$\|\Delta_{LST}\|$	(%)	t	Significance %
RCP4.5	24,500.00	10.40	0.84	>80%
RCP8.5	4500.00	1.75	-	NST
Middle Future (2061–2100)				
Scenario	$\|\Delta_{LST}\|$	(%)	t	Significance %
RCP4.5	34,000.00	12.70	0.70	>75%
RCP8.5	19,500.00	8.00	0.68	>75%
Future (2021–2100)				
Scenario	$\|\Delta_{LST}\|$	(%)	t	Significance %
RCP4.5	0.00	0.00	-	NST
RCP8.5	25,000.00	9.30	1.28	>85%

Note: NST: no significant trend.

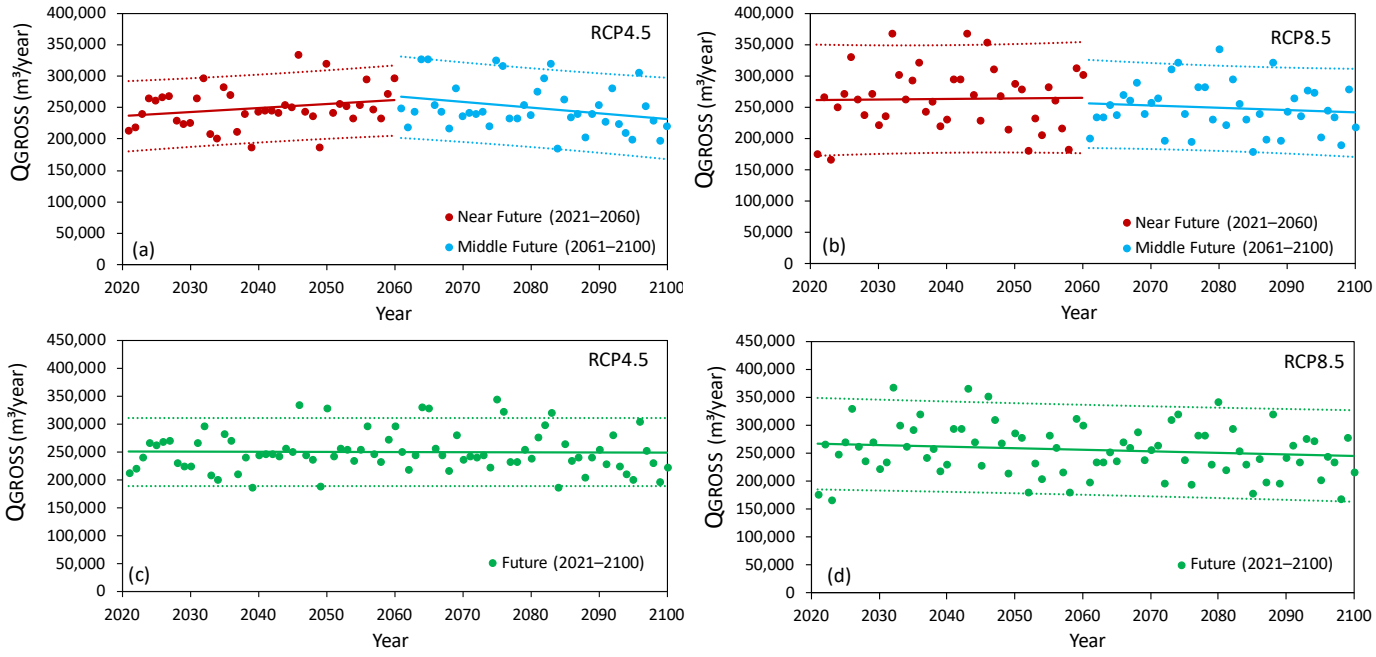


Figure 7. Inter-annual variations in the average gross LST rates for the near future, middle future, and whole future period. (**a**,**c**): RCP4.5 and (**b**,**d**): RCP8.5. Dotted lines represent the 90% confidence bound.

The near and middle future gross LST rates in the RCP4.5 scenario are nearly balanced, indicating no significant trend over the 80-year period, as shown in Table 4. Additionally, the decrease observed in the RCP8.5 scenario by the end of the 80 years has a significance level exceeding 85%. Results for both the RCP4.5 wave climate for the period 2021–2100 (Figure 8) and the RCP8.5 wave climate for the same period (Figure 9) are provided based on Kamphuis [33], Kaczmarek et al. [34], Bayram et al. [35], and LITDRIFT [37], presenting the trends of both swell- and wind-induced net and gross coastal sediment transport rates.

When examining the trends of net coastal sediment transport rates induced by both swell and wind waves for the RCP4.5 scenario, it can be observed that both swell- and wind-induced net coastal sediment transports show a decreasing trend. Analyzing the trend analysis of gross coastal sediment transport, it can be observed that swell-induced gross coastal sediment transports exhibit a decreasing trend, while wind-induced gross coastal sediment transport rates show an increasing trend, contrary to swell.

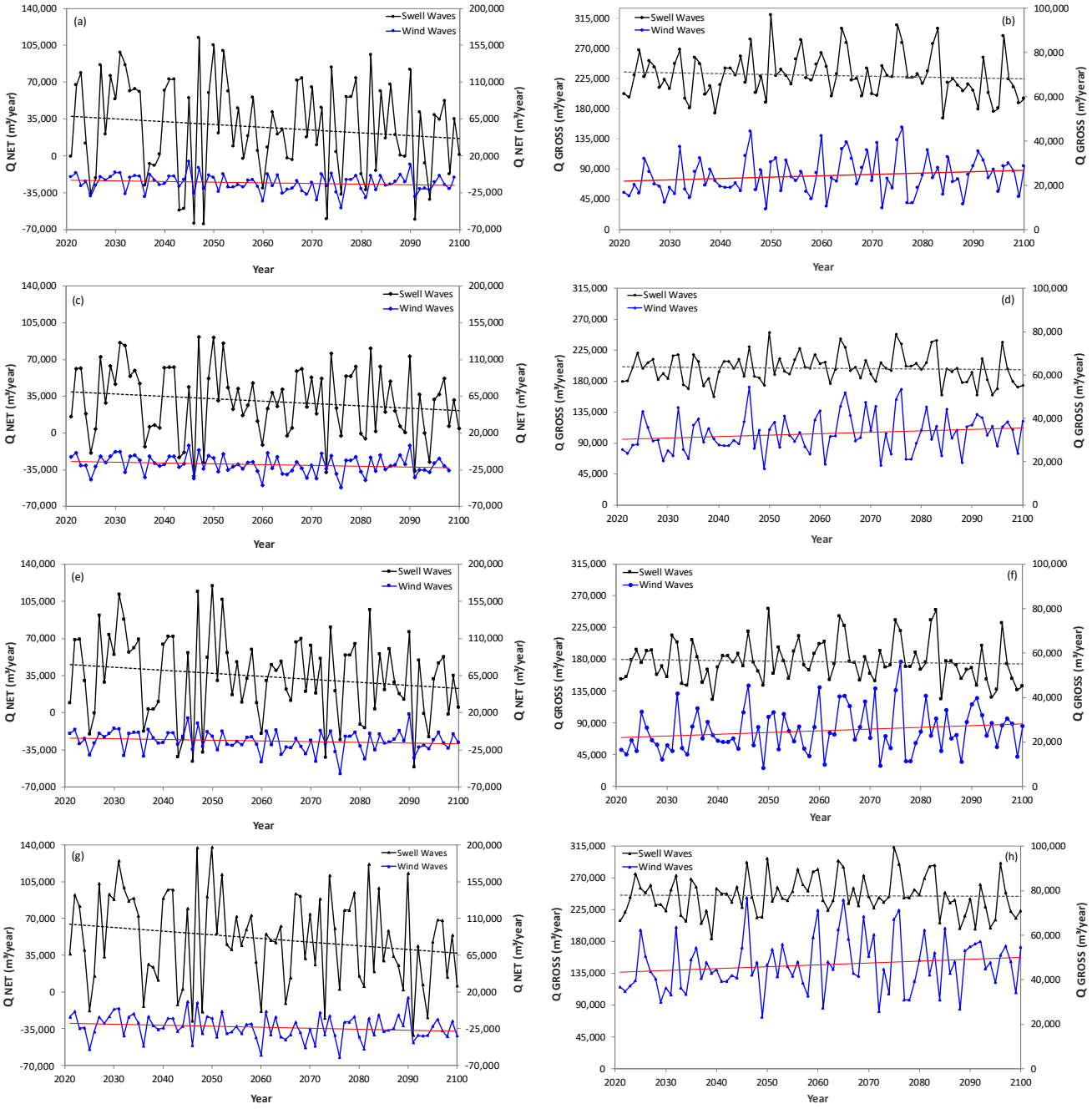


Figure 8. Annual net and gross longshore sediment transport rates based on the RCP4.5 scenario: Kamphuis [33]: (**a**) Q_{NET}, (**b**) Q_{GROSS}; Kaczmarek et al. [34]: (**c**) Q_{NET}, (**d**) Q_{GROSS}; Bayram et al. [35]: (**e**) Q_{NET}, (**f**) Q_{GROSS}; and LITDRIFT: (**g**) Q_{NET}, (**h**) Q_{GROSS}.

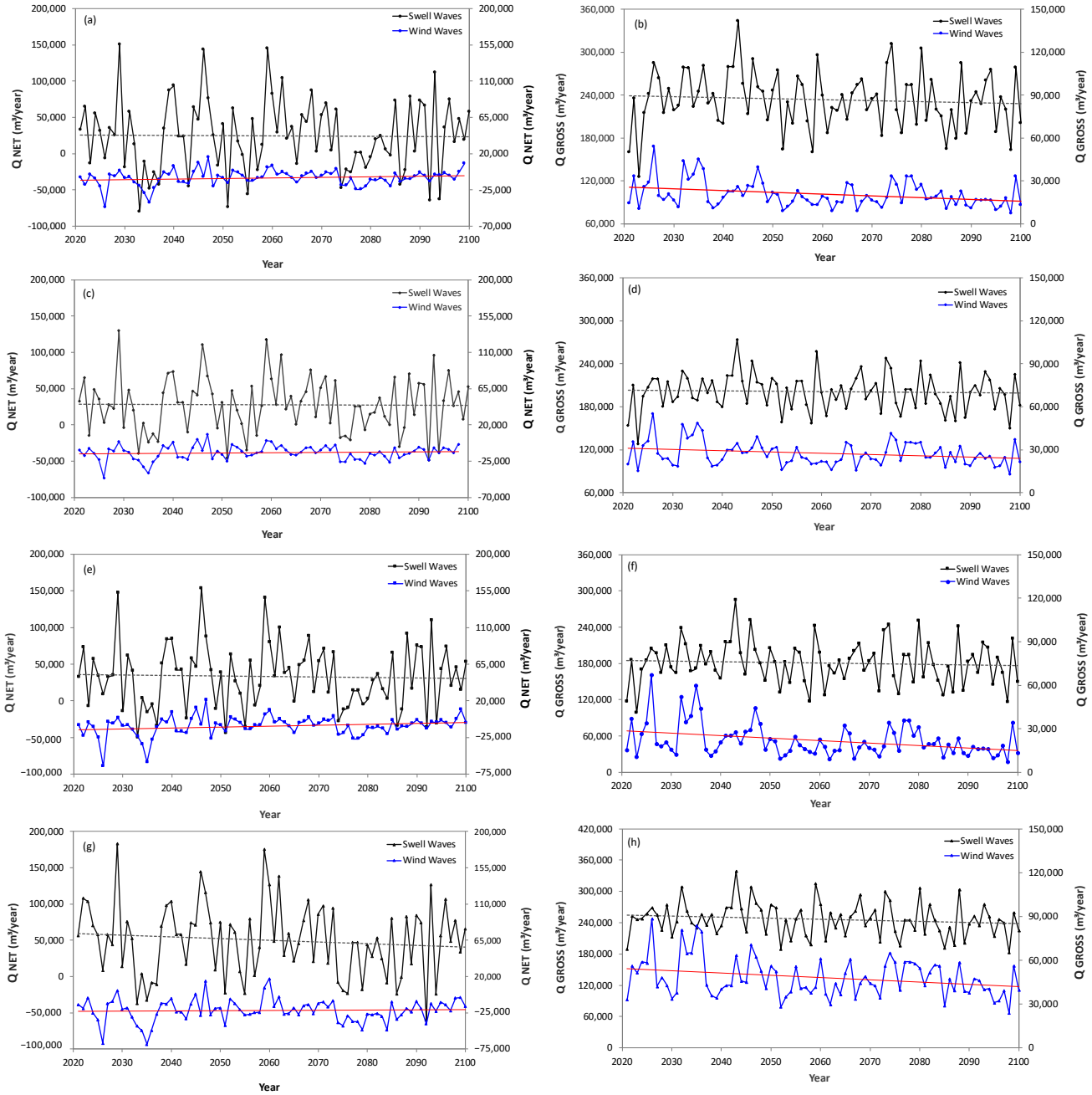


Figure 9. Annual net and gross longshore sediment transport rates based on the RCP8.5 scenario: Kamphuis [33]: (**a**) Q_{NET}, (**b**) Q_{GROSS}; Kaczmarek et al. [34]: (**c**) Q_{NET}, (**d**) Q_{GROSS}; Bayram et al. [35]: (**e**) Q_{NET}, (**f**) Q_{GROSS}; and LITDRIFT: (**g**) Q_{NET}, (**h**) Q_{GROSS}.

On the contrary, according to the results of the RCP8.5 scenario, when examining the trends of net coastal sediment transport rates induced by swell and wind waves, it can be observed that swell-induced net coastal sediment transport shows a slightly decreasing trend, while wind-induced net coastal sediment transport exhibits an increasing trend. Trend analysis of gross coastal sediment transport for both swell-induced and wind-induced cases reveals a decreasing trend. Additionally, the decreasing trend in gross coastal sediment transport induced by wind waves is of a larger magnitude compared to swell-induced transport, indicating a greater decrease.

Comparing the LST rates driven by swell and wind waves, from Figures 8 and 9, it is evident that, for the RCP4.5 scenario, the net and gross LST rates resulting from swell are approximately 2.5 and 7 times greater, respectively, than those resulting from wind waves

across all methods utilized in the study (Figure 8a–h). In the RCP8.5 scenario, these ratios are approximately three and eight for net and gross, respectively (Figure 9a–h).

Furthermore, upon examination of Figures 8 and 9, it becomes evident that the wind-induced net LST in both RCP4.5 and RCP8.5 climate scenarios predominantly trends towards the WNW (upstream). Predictions suggest that the net LST originating from swell waves will primarily occur towards the ESE (downstream) in both scenarios, but in certain years of the 80-year study period, net LST occurrences towards the WNW (upstream) are anticipated. Additionally, it is observed that WNW (upstream)-directed net LST will occur more frequently in the RCP8.5 climate scenario than in the RCP4.5 scenario.

4.3. Comparison with Historical Data

After analyzing the LST rates derived from the climate scenarios RCP4.5 and RCP8.5 for the 80-year span from 2021 to 2100, along with the LST rates from the past 40 years (1978–2018), as provided in Başaran and Arı Güner [28], it was observed that, in the projected climate scenarios, the average net LST rates decreased while the average gross LST rates increased (Table 5).

Table 5. Average net and gross LST rates for the historical and future periods.

Period	Average LST Rates (m^3/year)	
	Net	Gross
1979–2018 (Historical)	66,400	188,400
2021–2100 (RCP4.5)	48,000	250,000
2021–2100 (RCP8.5)	51,500	255,000

To evaluate these results, it is necessary to investigate the wave parameters over the past 40 years and the forthcoming 80-year period under the examined climate scenarios, along with their evolution during the study periods. According to Basaran and Arı Güner, the annual average significant wave height (H_s) from 1979 to 2018 was 0.92 m, with an annual mean peak wave period (T_p) of 5.53 s [28]. Waves reached the shore from the N-NNW sector at a 12° angle with respect to true north, forming a 6.5° angle with the shoreline's normal [28]. Nevertheless, in both climate scenarios studied for the upcoming 80-year span (RCP4.5 and RCP8.5), it can be determined that both the significant wave height and the peak wave period increase compared to the preceding 40 years. Furthermore, there is an observed tendency for waves to approach the shoreline's normal at a smaller angle (Table 6).

Table 6. Wave parameters for the historical and future periods.

Period	Wave Parameters		
	H_s (m)	T_p (s)	D_m (°)
Historical	0.92	5.53	12.0°
RCP4.5	0.94	5.74	15.2°
RCP8.5	0.95	5.75	17.5°

It is evident that the rise in both significant wave height and peak wave period, when compared to the past 40 years, within the RCP4.5 and RCP8.5 climate scenarios, led to the increase in the gross LST rates outlined in Table 4. While the observation that total waves approach the coast at a perpendicular angle in the future climate scenarios provides a partial explanation for this decrease, it is not entirely comprehensive. Therefore, the wave parameters in both climate scenarios were also individually examined in terms of swell and wind waves.

As previously stated, swell waves typically propagate from the west-northwest (WNW) to the east-southeast (ESE), resulting in downstream transport in both the studies

by Başaran and Arı Güner [28] and the current research. Conversely, wind waves exhibit the opposite pattern. When comparing past swell waves to those projected by climate scenarios, a slight decrease in the significant wave heights of swell waves was observed, leading to a reduction in downstream-directed net LST rates. Furthermore, within the RCP4.5 climate scenario, significant wave heights and peak wave periods tend to decrease for swell waves but increase for wind waves. This discrepancy amplifies the upstream-directed transport induced by wind waves, further lowering the net LST rates. In the case of the RCP8.5 climate scenario, while the significant wave heights of swell waves increase, peak wave periods decrease more substantially. Conversely, the significant wave heights of wind waves decrease while peak periods increase. This balance between the two parameters results in a smaller decrease in the net LST rates compared to the RCP4.5 climate scenario. In this way, while increases in the significant wave height and peak wave period of total waves cause an increase in the gross LST rates, there are decreases in the net LST rates due to the increase in wind-induced LST in future climate scenarios.

4.4. Assessment of Future Shoreline Change

Simulations were carried out to simulate the evolution of a 25.2 km shoreline section along the Karasu Coast over an 80-year period (2021–2100). The key findings from the shoreline change model (LITLINE), driven by wave and sediment data derived from the RCP4.5 and RCP8.5 scenarios, are as follows:

The study area exhibits an annual average net longshore sediment transport (LST) of approximately 48,000 and 51,500 m^3/year for the RCP4.5 and RCP8.5 scenarios, respectively (Table 3). With Karasu being an active coast, any structural intervention in the coastal area would inevitably result in deformations. Sediment transport along the coast within the study area primarily occurs from west-northwest (WNW) (upstream) to east-southeast (ESE) (downstream). The model results indicate an average annual maximum erosion of −0.5 m for the period 2021–2060 for both RCP4.5 and RCP8.5 scenarios (see Figure 10a,b and Table 7). For the subsequent period of 2061–2100, the average annual maximum erosion is determined to be −0.1 m for both scenarios. The overall average annual maximum erosion for the entire period from 2021 to 2100 is calculated as −0.26 m for both RCP4.5 and RCP8.5. Regarding annual average maximum accretion, the model results show values of +6.5 m and +4.9 m for the RCP4.5 and RCP8.5, respectively, for the period 2021–2060 (Figure 10a,b and Table 7). The location of maximum accretion is immediately west of the river mouth. For the subsequent period of 2061–2100, the annual average maximum accretion is +2.6 m and +2.0 m for the RCP4.5 and RCP8.5, respectively, with the maximum accretion location remaining unchanged. Over the entire period from 2021 to 2100, the annual average maximum accretion is determined to be +4.6 m and +3.4 m for the RCP4.5 and RCP8.5, respectively. Notably, there is no significant difference in erosion along the Karasu Coast between the near future (2021–2060) and middle future (2061–2100) for both scenarios. However, when examining accretion, it can be observed that there is significantly higher accretion in the near future (2021–2060), followed by an approximately 2.5-fold decrease in the middle future (2061–2100) for both scenarios. In the middle future (2061–2100), the shoreline exhibits greater stability in terms of erosion and accretion, which is attributed to the decreasing trend in gross sediment transport, as shown in Figure 6.

Table 7. Annual average erosion and accretion rates according to the RCP4.5 and RCP8.5 climate scenarios.

Wave Climate Scenario	Period	Maximum Erosion (m^3/year)	Maximum Accretion (m^3/year)
RCP4.5	2021–2060	0.50	6.50
	2061–2100	0.10	2.60
	2021–2100	0.26	4.60
RCP8.5	2021–2060	0.50	4.90
	2061–2100	0.10	2.00
	2021–2100	0.26	3.40

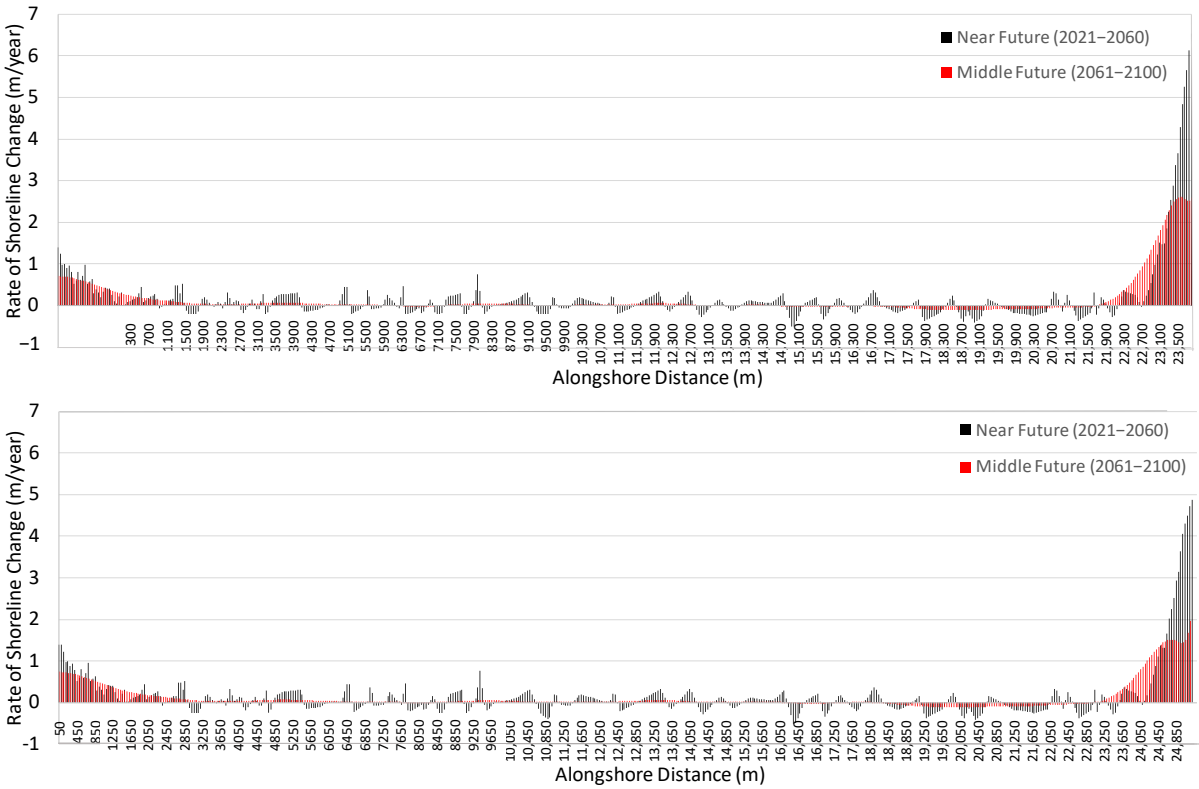


Figure 10. Annual rates of shoreline change according to (**upper**) RCP4.5 and (**lower**) RCP8.5.

In Figure 11, the shorelines obtained for the years 2060 and 2100 are depicted according to the RCP4.5 scenario (Figure 11a) and the RCP8.5 scenario (Figure 11b). As seen in Table 7 and Figure 11, accretion occurs on the shoreline as a result of LST in both RCP4.5 and RCP8.5 climate scenarios during the 80-year study period. When the changes occurring on the shoreline in both climate scenarios are examined for the near future and middle future, it is noticeable that there is more accretion in the near future, while this amount decreases in the middle future, as evident from the results provided in Table 7. This case can be explained by the fact that, in both climate scenarios, wave parameters tend to increase in the near future and decrease in the middle future. While the increases in wave height and period in the near future will cause the gross LST rate occurring along the Karasu Coast to increase, the decrease in these parameters in the middle future will cause the accretion amount on the shoreline to increase due to the decreasing gross LST (Tables 2 and 7).

Additionally, when evaluating shoreline changes, specifically for the RCP4.5 and RCP8.5 climate scenarios, the amount of accretion in the RCP4.5 scenario exceeds that in the RCP8.5 scenario. As depicted in Table 7, greater accretion is observed in the RCP4.5 scenario than in the RCP8.5 scenario, both in the near future and middle future. This discrepancy can be attributed to the trends in wave parameters during the near and middle futures. Specifically, while wave height and period exhibit more pronounced increases in the near future in the RCP4.5 scenario, there is a greater decrease in wave height, especially in the middle future, in the RCP4.5 scenario compared to the RCP8.5 scenario.

Furthermore, upon examining the net LST rates for near and middle future periods, it was observed that there is a decrease of approximately 23% in the middle future compared to the near future in both climate scenarios. Therefore, there is a greater accretion of the shoreline in the near future than in the middle future for both climate scenarios.

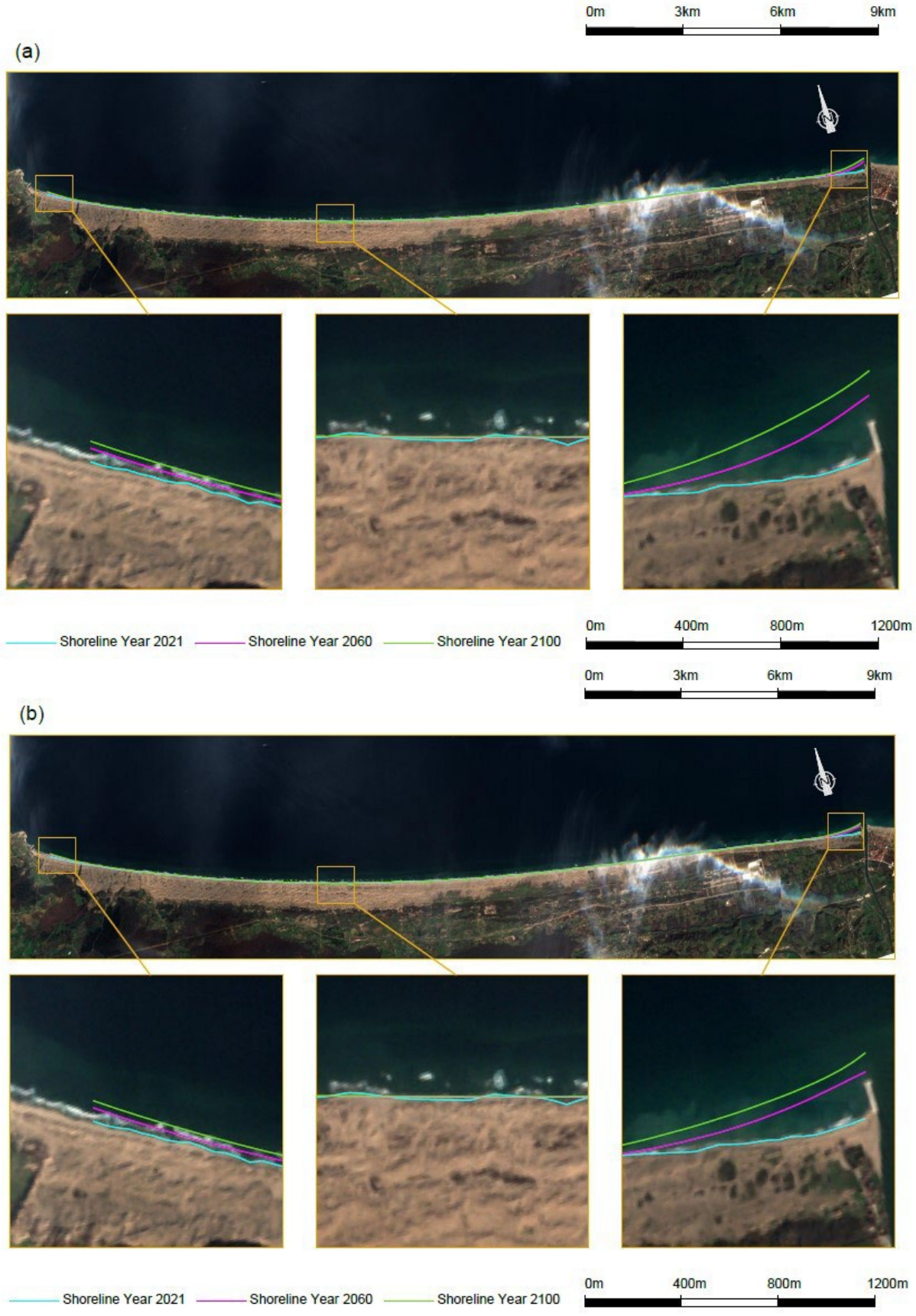


Figure 11. Projected shorelines between 2021 and 2100 according to (**a**) RCP4.5 and (**b**) RCP8.5.

5. Discussion

In this study, our future wave climate analysis, including the RCP4.5 and RCP8.5 climate scenario and the longshore sediment transport evaluation for the future period on the Karasu Coast, ensures significant and necessary results for coastal management processes.

The results show that, for the RCP4.5 wave climate scenario, the annual average wave characteristics in the study area are H_s = 0.94 m and T_p = 5.74 s, and the waves predominantly approach the coast from the north-northeast (N-NE) at a 15° angle with respect to true north; in the RCP8.5 climate scenario, the results reveal that these parameters are 0.95 m, 5.75 s, and 17.5° (N-NE), respectively. The annual net and gross LST rates were calculated for each scenario using empirical and numerical methods (Kamphuis [33], Kaczmarek et al. [34], Bayram et al. [35], and LITDRIFT [37]).

Seasonal variations show that higher wave heights are observed in the autumn and winter months, leading to increased LST rates due to the stronger wave action. Conversely, lower wave heights in the spring and summer seasons result in reduced LST rates.

Analyzing the 80-year changes reveals that, in both scenarios, significant wave heights increase, wave periods decrease, and waves shift eastward, approaching the shoreline's normal. Wave heights increase more in the RCP8.5 climate scenario with a greater eastward shift, leading to larger LST transports by the end of the 80 years.

The findings of this study are important for coastal management in the Karasu region. As changing wave climates can alter sediment transport processes, as noted by Bonaldo et al. [3], it is anticipated that variations in wave heights and directions on the Karasu Coast will significantly impact coastal erosion and accretion. This will facilitate an integrated management approach to wave climate and LST patterns in future planning for the Karasu Coast. For example, this study indicates that larger LST rates will occur under the RCP8.5 climate scenario, suggesting a more dynamic shoreline and coastal morphology and necessitating appropriate measures along the coast.

According to the RCP4.5 and RCP8.5 climate scenarios, the LITLINE model was used to separately analyze the evolution of the Karasu shoreline in the near future (2021–2060) and the middle future (2061–2100), in addition to assessing the LST rates projected for the end of the 80-year period. In both climate scenarios, the amount of erosion is similar, but the amount of accretion varies between the near and middle future. Significant accretion is expected west of the Sakarya River in both scenarios, with the RCP4.5 scenario showing a more pronounced rate of accretion compared to the RCP8.5 scenario.

Comparing wave data between historical records and projections under the RCP4.5 and RCP8.5 climate scenarios reveals that future wave conditions are anticipated to be higher and more energetic, aligning with global climate change predictions. However, the most notable difference between historical and future wave data lies in the eastward shift of mean wave direction in the projected scenarios. This shift is expected to alter the direction of longshore sediment transport (LST).

This study represents the initial long-term predictions of longshore sediment transport (LST) variability using future wave climate projections along the southwestern Black Sea. Despite the uncertainties and methodological limitations in estimating LST rates discussed in this paper, this study and its findings can serve as valuable tools for long-term assessments of beach behavior and coastal protection strategies.

6. Conclusions

The Karasu coast selected as the study area is 25 km long and has a dynamic sediment transport mechanism including both of longshore and cross-shore sediment transport. This study aims to present possible changes in longshore sediment transport rates and patterns owing to variations in wave climate parameters based on the RCP4.5 and RCP8.5 wave climate scenarios as a result of global climate change, through different empirical and numerical models. This study also reveals the long-term shoreline changes along the Karasu coast using the LITLINE numerical model.

The dominant wave directions resulted in an easterly net LST, which was computed using various empirical and numerical methods. The swell wave-induced gross LST is an order of magnitude higher than the wind-induced gross LST by a factor of 7 (8) in the RCP4.5 (RCP8.5). The swell wave-induced net LST is an order of magnitude higher than the wind-induced net LST by a factor of 2.5 (3) in the RCP4.5 (RCP8.5) due to the existence of significant fetch distances (>600 km) that influence the generation of swell waves within the Black Sea Basin.

At the end of 80 years, the net LST rate decreased by ~400 m^3/year and ~50 m^3/year (average of 80 years) according to the RCP4.5 and RCP8.5 scenarios, respectively. The net and gross LST rates obtained in the RCP8.5 climate scenario were found to be 1.08 and 1.02 times greater, respectively, compared to the RCP4.5 scenario. This is attributed to the higher wave heights with a greater eastward shift in the RCP8.5 climate scenario. In the near future, the net LST rate for the RCP4.5 scenario will have a greater increasing trend compared to the RCP8.5 scenario. This trend is associated with greater wave heights in the RCP4.5 scenario and the fact that the RCP8.5 scenario has a smaller wave angle in relation to the shoreline's normal.

During the study period, divided into near future (2021–2060) and middle future (2061–2100) periods, the gross LST shows varying trends. In the near future period, there is an average increase of 10.4% (1.75%) in the RCP4.5 (RCP8.5) scenario, which is associated with increases in both significant wave heights and peak wave periods. Conversely, during the middle future period (2061–2100), the gross LST rates decrease by an average of 12.7% (8.0%) in the RCP4.5 (RCP8.5) scenario, attributed to decreases in both significant wave heights and peak wave periods in both climate scenarios.

The gross LST rates in the near and middle future under the RCP4.5 scenario nearly offset each other. In contrast, under the RCP8.5 scenario, there is an imbalance due to the decrease in LST rates during the middle future period. This discrepancy can be attributed to the fact that the rates of increase and decrease in the wave parameters in the RCP4.5 wave climate scenario for the near and middle future periods are comparable, whereas in the RCP8.5 wave climate scenario, the rate of increase in wave parameters in the near future does not correspond with the rate of decrease in the middle future. This condition results in larger changes in LST rates during the near and middle future periods of the RCP4.5 climate scenario compared to the RCP8.5 climate scenario, contrary to the trends observed over the 80-year period.

In the projected climate scenarios, when compared to historical data (1978–2018), there is an increase in average gross longshore sediment transport (LST) rates despite a decrease in average net LST rates. This increase in gross LST rates can be attributed to the higher significant wave heights and longer peak wave periods observed in both climate scenarios. The decrease in net LST rates is primarily explained by a slight reduction in the significant wave heights of swell waves over the past 40 years, coupled with an increase in the significant wave heights of wind waves. Consequently, there has been an increase in LST towards the west-northwest (WNW) direction, while LST towards the east-southeast (ESE) direction has decreased. This directional shift has resulted in a net reduction in LST rates in the climate scenarios compared to historical LST rates.

Since the increase and decrease rates in wave parameters are greater in the RCP4.5 scenario than the RCP8.5 scenario, the maximum rate of accretion along the Karasu Coast is 1.4 times higher in the RCP4.5 climate scenario compared to the RCP8.5 scenario. There is no significant difference in erosion between the two climate scenarios, with shoreline erosion showing very close patterns to each other in both near and middle future periods under both scenarios. However, there is greater accretion anticipated in the near future than in the middle future due to the expected increase in wave parameters in the near future, followed by a decrease in the middle future. Specifically, the accretion rate is 2.5 times higher in the near future compared to the middle future.

Author Contributions: Conceptualization, B.B. and H.A.A.G.; methodology, B.B. and H.A.A.G.; software, H.A.A.G.; validation, B.B. and H.A.A.G.; formal analysis and investigation, B.B.; writing—original draft preparation, B.B. and H.A.A.G.; writing—review and editing, H.A.A.G.; visualization, B.B.; supervision, H.A.A.G.; project administration, H.A.A.G. All authors have read and agreed to the published version of the manuscript.

Funding: This study was supported by the Scientific and Technological Research Council of Turkey (TUBITAK) under Grant Number 111Y333. The authors would like to thank the TUBITAK for their support.

Data Availability Statement: The data will be made available upon request.

Conflicts of Interest: The authors declare no conflicts of interest.

Appendix A

This study conducted a Student's *t*-test to assess the presence of a statistically significant linear trend in longshore sediment transport (LST) along the southwestern coast of the Black Sea, specifically the Karasu Coast.

The residuals of regression, e, are defined as $e = (a_0 + a_1 x) - y$, and their variance, s_e^2, is given by Santer et al. [39].

$$s_e^2 = -\frac{1}{N_{eff} - 2}\sum_i^N e_i^2 \quad \text{(A1)}$$

N_{eff} is the effective sample size. The standard error of the regression coefficient, and sa, are shown to follow [39].

$$s_a^2 = -\frac{s_e^2}{\sum_i^N (x - \overline{x})^2} \quad \text{(A2)}$$

The statistic, $t = a_1/s_a$, is distributed as Student's t, and the calculated t value is compared with a critical t value for a stipulated significance level α and $N_{eff} - 2$ degrees of freedom.

References

1. Adams, P. Effect of climate change and wave direction on longshore sediment transport patterns in Southern California. *Clim. Chang.* **2011**, *109*, 211–228. [CrossRef]
2. Almar, R.; Kestenare, E.; Reyns, J.; Jouanno, J.; Anthony, E.J.; Laibi, R.; Hemer, M.; Du Penhoat, Y.; Ranasinghe, R. Response of the Bight of Benin (Gulf of Guinea, West Africa) Coastline to Anthropogenic and Natural Forcing, Part1: Wave Climate Variability and Impacts on the Longshore Sediment Transport. *Cont. Shelf Res.* **2015**, *110*, 48–59. [CrossRef]
3. Bonaldo, D.; Benetazzo, A.; Sclavo, M.; Carniel, S. Modelling Wave-Driven Sediment Transport in a Changing Climate: A Case Study for Northern Adriatic Sea (Italy). *Reg. Environ. Chang.* **2015**, *15*, 45–55. [CrossRef]
4. Casas-Prat, M.; Wang, X.L.; Swart, N. CMIP5-Based Global Wave Climate Projections Including the Entire Arctic Ocean. *Ocean Model.* **2016**, *123*, 66–85. [CrossRef]
5. Dastgheib, A.; Reyns, J.; Thammasittirong, S.; Weesakul, S.; Thatcher, M.; Ranasinghe, R. Variations in the Wave Climate and Sediment Transport due to Climate Change Along the Coast of Vietnam. *J. Mar. Sci. Eng.* **2016**, *4*, 86. [CrossRef]
6. Fernández-Fernández, S.; Silva, P.A.; Ferreira, C.C.; Carracedo-García, P.E. Longshore Sediment Transport Estimation at Areão Beach (NW Portugal) under Climate Change Scenario. *J. Coast. Res.* **2020**, *95*, 479–483. [CrossRef]
7. Chowdury, P.; Behera, M.R.; Reeve, D.E. Future Wave-Climate Driven Longshore Sediment Transport Along the Indian Coast. *Clim. Chang.* **2020**, *162*, 405–424. [CrossRef]
8. Dickson, M.E.; Kench, P.S.; Kantor, M.S. Longshore Transport of Cobbles on a Mixed Sand and Gravel Beach, Southern Hawke Bay, New Zealand. *Mar. Geol.* **2007**, *287*, 31–42. [CrossRef]
9. Zacharioudaki, A.; Reeve, D.E. Shoreline Evolution Under Climate Change Wave Scenarios. *Clim. Chang.* **2011**, *108*, 73–105. [CrossRef]
10. Rajasree, B.R.; Deo, M.C.; Sheela Nair, L. Effect of Climate Change on Shoreline Shifts at a Straight and Continuous coast. *Estuar. Coast. Shelf Sci.* **2016**, *183*, 221–234. [CrossRef]
11. Suursaar, I.; Tnisson, H.; Alari, V.; Raudsepp, U. Projected Changes in Wave Conditions in the Baltic Sea by the end of 21st Century and the Corresponding Shoreline Changes. *J. Coast. Res.* **2016**, *75*, 1012–1016. [CrossRef]
12. Enríquez, A.R.; Marcos, M.; Álvarez-Ellacuría, A.; Orfila, A.; Gomis, D. Changes in Beach Shoreline due to Sea Level Rise and Waves Under Climate Change Scenarios: Application to the Balearic Islands (Western Mediterranean). *Nat. Hazards Earth Syst. Sci.* **2017**, *17*, 1075–1089. [CrossRef]

13. Gopikrishna, B.; Deo, M.C. Changes in the Shoreline at Paradip Port, India in Response to Climate Change. *Geomorphology* **2018**, *303*, 243–255. [CrossRef]
14. Rajasree, B.R.; Deo, M.C. Future Geomorphologic Changes under the Changing Climate. *J. Coast. Res.* **2020**, *89*, 7–14. [CrossRef]
15. Alvarez-Cuesta, M.; Toimil, A.; Losada, I.J. Modelling Long-Term Shoreline Evolution in Highly Anthropized Coastal Areas. Part 2: Assessing the Response to Climate Change. *Coast. Eng.* **2021**, *169*, 103985. [CrossRef]
16. D'Anna, M.; Idier, D.; Castelle, B.; Rohmer, J.; Cagigal, L.; Mendez, F.J. Effects of Stochastic Wave Forcing on Probabilistic Equilibrium Shoreline Response Across the 21st Century Including Sea-Level Rise. *Coast. Eng.* **2021**, *175*, 104149. [CrossRef]
17. Santiago, I.; Camus, P.; Gonzalez, M.; Liria, P.; Epelde, I.; Chust, G.; Campo, A.; Uriarte, A. Impact of Climate Change on Beach Erosion in the Basque Coast (NE Spain). *Coast. Eng.* **2021**, *167*, 103916. [CrossRef]
18. Dastgheib, A.; Martinez, C.; Udo, K.; Ranasinghe, R. Climate Change Driven Shoreline Change at Hasaki Beach Japan: A Novel Application of the Probabilistic Coastline Recession (PCR) Model. *Coast. Eng.* **2022**, *172*, 104079. [CrossRef]
19. Chowdury, P.; Behera, M.R. Effect of Long-Term Wave Climate Variability on Longshore Sediment Transport Along Regional Coastlines. *Prog. Oceanogr.* **2017**, *156*, 145–153. [CrossRef]
20. Chowdhury, P.; Behera, M.R. Evaluation of CMIP5 and CORDEX Derived Wave Climate in Indian Ocean. *Clim. Dyn.* **2018**, *52*, 4463–4482. [CrossRef]
21. Splinter, K.D.; Davidson, M.A.; Golshani, A.; Tomlinson, R. Climate Controls on Longshore Sediment Transport. *Cont. Shelf Res.* **2012**, *48*, 146–156. [CrossRef]
22. Samaras, A.G.; Koutitas, C.G. Modeling the Impact of Climate Change on Sediment Transport and Morphology in Coupled Watershed-Coast Systems: A Case Study Using an Integrated Approach. *Int. J. Sediment Res.* **2014**, *29*, 304–315. [CrossRef]
23. Ranasinghe, R.; Callaghan, D.; Stive, M.J.F. Estimating Coastal Recession due to Sea Level Rise: Beyond the Bruun Rule. *Clim. Chang.* **2012**, *110*, 561–574. [CrossRef]
24. Ranasinghe, R.; Duong, T.; Uhlenbrook, S.; Roelvink, D.; Stive, M. Climate Change Impact Assessment for Inlet-Interrupted Coastlines. *Nat. Clim. Chang.* **2013**, *3*, 83–87. [CrossRef]
25. Ashton, A.D.; Donnelly, J.P.; Evans, R.L. A Discussion of the Potential Impacts of Climate Change on the Shorelines of the Northeastern USA. *Mitig. Adapt. Strategies Glob. Chang.* **2008**, *13*, 719–743. [CrossRef]
26. Vitousek, S.; Barnard, P.L.; Fletcher, C.H.; Frazer, N.; Erikson, L.; Storlazzi, C.D. Doubling of Coastal Flooding Frequency within Decades due to Sea-Level Rise. *Sci. Rep.* **2017**, *7*, 1399. [CrossRef] [PubMed]
27. Field, C.B.; Barros, V.R.; Dokken, D.J.; Mach, K.J.; Mastrandrea, M.D. Coastal Systems and Low-Lying Areas in Climate Change 2014 Impacts, Adaptation, and Vulnerability. In *IPCC 2014*; Cambridge University Press: Cambridge, UK, 2014; pp. 361–410.
28. Basaran, B.; Guner, H.A. Effect of Wave Climate Change on Longshore Transport in Southwestern Black Sea. *Estuar. Coast. Shelf Sci.* **2021**, *258*, 107415. [CrossRef]
29. Avşar, N.B. Sea Level Changes in the Black Sea and Its Impacts on the Coastal Areas. Ph.D. Thesis, Zonguldak Bülent Ecevit University, Zonguldak, Türkiye, 2019.
30. Divinsky, B.V.; Kosyan, R.D. Spatio Temporal Variability of the Black Sea Wave Climate in the Last 37 Years. *Cont. Shelf Res.* **2017**, *136*, 1–19. [CrossRef]
31. Islek, F.; Yuksel, Y.; Sahin, C. Evaluation of Regional Climate Models and Future Wave Characteristics in an Enclosed Sea: A Case Study of the Black Sea. *Ocean Eng.* **2022**, *262*, 112220. [CrossRef]
32. Islek, F.; Yuksel, Y.; Sahin, C. Evaluation of Regional Climate Models and Future Wind Characteristics in the Black Sea. *Int. J. Climatol.* **2021**, *42*, 1877–1901. [CrossRef]
33. Kamphuis, J.W. Alongshore Sediment Transport Rate. *J. Waterw. Port Coast. Ocean Eng.* **1991**, *117*, 624–640. [CrossRef]
34. Kaczmarek, L.M.; Ostrowski, R.; Pruszak, Z.; Rozynski, G. Selected Problems of Sediment Transport and Morphodynamics of a Multi-Bar Nearshore Zone. *Estuar. Coast. Shelf Sci.* **2005**, *62*, 415–425. [CrossRef]
35. Bayram, A.; Larson, M.; Hanson, H. A New Formula for the Total Longshore Sediment Transport Rate. *Coast. Eng.* **2007**, *54*, 700–710. [CrossRef]
36. DHI. *LITPACK-Noncohesive Sediment Transport in Currents and Waves, User Guide*; DHI Water and Environment: Hersholm, Denmark, 2016.
37. DHI. *LITDRIFT Longshore Current and Littoral Drift, User Guide*; DHI Water and Environment: Hersholm, Denmark, 2016.
38. DHI. *LITLINE Coastline Evolution, User Guide*; DHI Water and Environment: Hersholm, Denmark, 2016.
39. Santer, B.D.; Wigley, T.M.L.; Boyle, J.S.; Gaffen, J.S.; Hnilo, J.J.; Nychka, D.; Parker, D.E.; Taylor, K.E. Statistical Significance of Trends and Trend Differences in Layer-Average Atmospheric Temperature Time Series. *J. Geophys. Res.* **2000**, *105*, 7337–7356. [CrossRef]

Disclaimer/Publisher's Note: The statements, opinions and data contained in all publications are solely those of the individual author(s) and contributor(s) and not of MDPI and/or the editor(s). MDPI and/or the editor(s) disclaim responsibility for any injury to people or property resulting from any ideas, methods, instructions or products referred to in the content.